

STORM: SYNERGISTIC CROSS-SCALE SPATIO-TEMPORAL MODELING FOR WEATHER FORECASTING

Qihe Huang¹, Zhengyang Zhou^{1,2,*}, Yangze Li¹, Jiaming Ma¹, Kuo Yang¹, Binwu Wang^{1,2},
Xu Wang^{1,2}, Yang Wang^{1,2,*}

¹University of Science and Technology of China (USTC), Hefei, Anhui, China

²Suzhou Institute for Advanced Research, USTC, Suzhou, Jiangsu, China

hqh@mail.ustc.edu.cn

ABSTRACT

Accurate weather forecasting is crucial for climate research, disaster mitigation, and societal planning. Despite recent progress with deep learning, global atmospheric data remain uniquely challenging since weather dynamics evolve across heterogeneous spatial and temporal scales ranging from planetary circulations to localized phenomena. Capturing such cross-scale interactions within a unified framework remains an open problem. To address this gap, we propose **STORM**, a synergistic cross-scale spatio-temporal model that disentangles atmospheric variations into multiple scales to uncover scale-specific dependencies. In addition, it enables coherent forecasting across multiple resolutions, maintaining consistent temporal evolution. Experiments on benchmark datasets demonstrate that STORM consistently delivers superior performance across both global and regional settings, as well as for short- and long-term forecasts. The code is available at <https://github.com/h505023992/STORM>.

1 INTRODUCTION

Accurate weather forecasting plays a pivotal role in climate research, disaster mitigation, and supporting decision-making in agriculture, energy, and public safety (Kuligowski & Barros, 1998; Baboo & Shereef, 2010; Lam et al., 2022; Gao et al., 2025). Traditional Numerical Weather Prediction (NWP) systems (Bauer et al., 2015) are grounded in the numerical solution of atmospheric dynamics (Bucciotti et al., 2023), ensuring physical consistency across scales (Achatz et al., 2024). However, with the rapid growth of observational data and the demand for high-resolution, long-horizon forecasts, NWP approaches are increasingly constrained by high computational costs and difficulties in leveraging data-driven knowledge at scale (Rasp et al., 2023).

Deep learning (DL) has recently emerged as a promising paradigm for spatio-temporal forecasting (Yu et al., 2018; Wu et al., 2019; Guo et al., 2022; Wang et al., 2024a; Ma et al., 2025c;b;a;d;f;e; 2026a;b; Huang et al., 2025b;a;c; 2024a;c; Lin et al., 2023). Early efforts, such as ConvLSTM (Shi et al., 2015) and PredRNN (Wang et al., 2017), demonstrated the potential of neural architectures for regional precipitation prediction. More recent large-scale weather models, such as Pangu-Weather (Bi et al., 2023), GraphCast (Lam et al., 2022), and FourCastNet (Pathak et al., 2022), have achieved impressive advances in global forecasting and even in predicting extreme events (Chen et al., 2023b). Despite these successes, current DL-based approaches still face several critical limitations: **❶ Multi-scale heterogeneity.** Global atmospheric circulation evolves at coarse scales, while regional variability emerges at finer scales. Balancing these dynamics within a single model remains challenging (Zhou et al., 2023). **❷ Diverse temporal evolution.** Distinct scales exhibit different temporal dynamics, and existing models struggle to learn coherent cross-scale evolution, often leading to degraded performance in long-term forecasts (Wang et al., 2024b). **❸ Weak cross-scale interaction.** Most methods process different spatial or temporal scales independently, overlooking their complementary roles and the synergistic effects across scales (Huang et al., 2024b). To address these challenges, we propose **STORM**, a synergistic cross-scale spatio-temporal method for accurate weather forecasting. As shown in Figure 1, STORM explicitly disentangles atmospheric variations across fine-to-coarse

*Zhengyang Zhou and Yang Wang are corresponding authors.

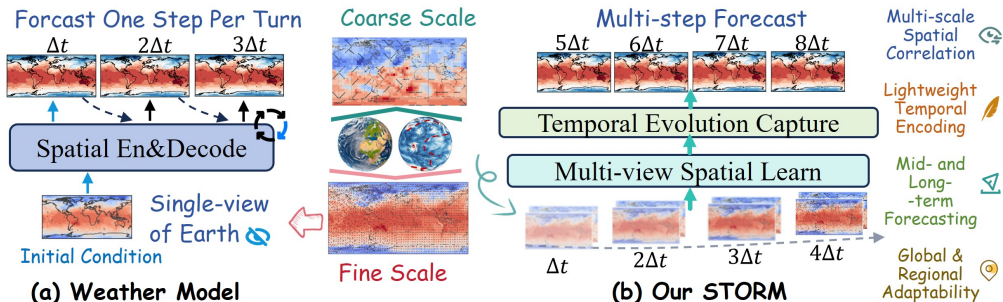


Figure 1: Comparison of main stream weather forecasting model and our STORM.

resolutions and integrates them via a cross-scale collaboration mechanism with temporal evolution learning. This design enables the model to capture global circulation patterns while preserving local high-frequency details, thereby enhancing both short- and long-term predictive skill. Through extensive experiments on benchmark meteorological datasets, we demonstrate that STORM achieves state-of-the-art forecasting performance. Our main contributions are summarized as follows:

- To address the challenge scale coupling in atmospheric data, we propose the first spatio-temporal modeling framework for weather forecasting. In particular, (i) it emphasizes cross-scale spatial learning to capture both unique local patterns and shared dependencies across different spatial resolutions, and (ii) it focuses on multi-step temporal evolution, rather than merely learning a single-step mapping from past to future states.
- We introduce STORM, a unified spatio-temporal framework for weather forecasting. It comprises (i) a *Hierarchical Earth Embedder* to build multi-resolution representations, (ii) a *Scale-Bridging Spatio-Temporal Encoder* to jointly model temporal evolution and spatial interactions across scales, and (iii) a *Level-Aligned Forecasting Decoder* to generate coherent multi-scale future predictions, enabling accurate decomposition, integration, and reconstruction of atmospheric dynamics.
- Extensive experiments on ERA5 datasets at multiple spatial resolutions (5.625° , 1° , and 0.25°) show that STORM consistently outperforms existing baselines across both global and regional domains. The framework demonstrates superior accuracy for short-term (hours) as well as long-term (several days) forecasts, effectively capturing fine-scale local patterns, medium-scale regional structures, and large-scale planetary circulations.

2 RELATED WORK

Global Weather Forecasting Global weather forecasting has seen rapid progress with the adoption of deep learning models [Weyn et al. \(2021\)](#); [Nguyen et al. \(2023\)](#). FourCastNet ([Pathak et al., 2022](#)), built upon Fourier neural operators, achieves forecasts comparable to numerical methods like IFS while being orders of magnitude faster. Pangu-Weather ([Bi et al., 2023](#)), leveraging Swin Transformers with earth-specific location embeddings, surpasses NWP baselines and demonstrates strong scalability. GraphCast ([Lam et al., 2022](#)) advances further by introducing message-passing networks to efficiently capture global dependencies and improve accuracy. FuXi ([Chen et al., 2023b](#)) extends the forecasting horizon, delivering 15-day predictions at skill levels comparable to ECMWF operational systems. FengWu ([Chen et al., 2023a](#)) integrates multi information flow, enabling improved representation of different atmospheric dynamics. Despite these advances, most existing models are primarily designed to learn a mapping from the current state to the next-step state, which limits their ability to capture long-range temporal evolution and synergistic cross-scale interactions.

Spatio-Temporal Modeling Recent advances in time-series forecasting have significantly improved modeling capacity across diverse settings, including loss-function design ([Wang et al., 2026b; 2025c;b;a; 2026c; Qiu et al., 2025b](#)), architectural innovations spanning linear, MLP-, Transformer-, and graph-based models ([Wang et al., 2023b; 2026a; Yue et al., 2025; Qiu et al., 2025c; Wu et al., 2025b; Hu et al., 2025b](#)), exogenous and irregular multivariate modeling ([Li et al., 2026; Qiu et al., 2025d; Liu et al., 2026a;b](#)), probabilistic and multimodal forecasting ([Wu et al., 2025c; 2026](#)), as well as comprehensive benchmarking efforts ([Qiu et al., 2024; 2025a; Hu et al., 2025a](#)). Building upon these developments, research has progressively extended from temporal modeling to spatio-temporal

forecasting, where spatial interactions, graph structures, and cross-scale dynamics become central modeling challenges (Ma et al., 2025c; Hu et al., 2026). Deep learning approaches for spatio-temporal modeling mainly focus on two data forms: *graph-structured* and *grid-structured* data (Liang et al., 2025). While graph-based methods have also been explored for irregular domains (Zhang et al., 2022; Wang et al., 2023a; 2024a), grid-based modeling remains particularly suitable for global-scale atmospheric data due to its structured nature. Early approaches such as ConvLSTM (Shi et al., 2015) and PredRNN (Wang et al., 2017) explicitly model temporal dependencies through recurrent connections, achieving promising results on precipitation nowcasting. To improve efficiency, SimVP (Gao et al., 2022a) replaces recurrent structures with pure convolutional operators, demonstrating competitive performance on benchmark sequence modeling tasks. More recently, Transformer-based architectures have been introduced, with models such as Earthformer (Gao et al., 2022b) leveraging attention mechanisms on gridded climate data to enhance long-range spatio-temporal dependencies. However, these models are primarily designed as general-purpose spatio-temporal learners and lack specialized adaptations to the unique multi-scale dynamics of weather and climate systems.

3 PROBLEM DEFINITION

In this study, we formulate weather forecasting as a multi-step spatiotemporal forecasting problem. At each time step t , the meteorological state consists of surface variables \mathbf{S}_t and atmospheric variables \mathbf{A}_t across 13 pressure levels. We concatenate them along the channel dimension to form the combined input: $\mathbf{X}_t = [\mathbf{S}_t, \mathbf{A}_t] \in \mathbb{R}^{H \times W \times C}$, where $H \times W$ is the number of spatial grid locations, and $C = C_s + C_a$ is the total number of variables, with C_s and C_a denoting the numbers of surface and atmospheric variables, respectively. Our formulation is based on a history of T steps to directly forecast the next L steps. Specifically, given historical inputs $\mathbf{X}_{t-T+1:t}$, the model predicts the future $\hat{\mathbf{X}}_{t+1:t+L} = \text{Model}(\mathbf{X}_{t-T+1:t}; \Theta)$, where Θ denotes the model parameters. To support ultra-long forecasting horizons (far beyond L), we adopt a recursive rollout strategy. After generating the first L predictions, the most recent T predicted states are fed back as inputs to produce the next block of L forecasts, and this process is repeated. This block-wise multi-step forecasting significantly alleviates the error accumulation typical of purely autoregressive one-step methods, enabling stable and accurate long-horizon predictions.

4 METHODS

As illustrated in Fig. 2, we introduce STORM, a unified framework for multi-scale spatio-temporal forecasting. The design of STORM is motivated by the intrinsic hierarchical nature of atmospheric dynamics, where large-scale circulations and small-scale local processes interact across different temporal horizons. To capture such complex dependencies, STORM consists of three key components: (i) **Hierarchical Earth Embedder** that progressively downsamples raw observations to construct multi-resolution representations, (ii) **Scale-bridging Spatio-temporal Encoder** that jointly models temporal evolution and spatial interactions while enabling information propagation from fine- to coarse-grained levels, and (iii) **Level-Aligned Forecasting Decoder** that projects multi-scale representations into future prediction through depth-specific transposed convolutions. Together, these components allow STORM to effectively decompose, bridge, and reconstruct atmospheric dynamics across scales for accurate weather forecasting.

4.1 HIERARCHICAL EARTH EMBEDDER

Earth observation data inherently exhibit multi-scale characteristics: coarse scales capture large-scale circulation patterns, while fine scales reflect local variations and detailed structures. To effectively leverage information across these scales, we propose the *Hierarchical Earth Embedder* for multi-scale embedding of global meteorological features. Given input data $\mathbf{X} = [\mathbf{S}, \mathbf{A}] \in \mathbb{R}^{T \times H \times W \times C}$, where T denotes the historical length, C represents the total number of surface and atmospheric variables, and $H \times W$ defines a fine-grained global grid, the data contains rich local details but makes it challenging to directly capture coarse-scale circulation and large-scale dependencies. To address this, we adopt a progressive, layer-wise downsampling strategy for multi-scale modeling and embedding.

First, a 3×3 spatial convolution is applied to the original fine-grained input to obtain the initial embedding $\mathbf{H}_0 \in \mathbb{R}^{T \times H \times W \times D}$, where D is the hidden embedding dimension. This step allows the

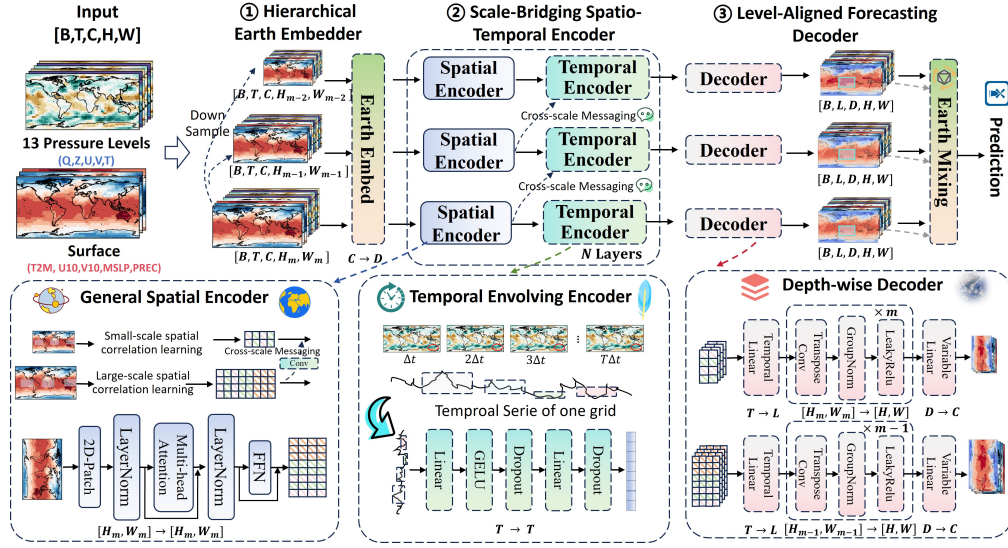


Figure 2: Illustration of the multi-scale collaborative meteorological forecasting model.

model to learn localized spatial representations while embedding the raw data. Subsequently, a series of strided convolutional layers with stride 2 are applied to progressively downsample the embeddings and capture increasingly coarser spatial structures:

$$\mathbf{H}_m = \text{LeakyReLU}(\text{GroupNorm}(\text{Conv2d}(\mathbf{H}_{m-1}; \text{kernel} = 3, \text{stride} = 2))), \quad (1)$$

where LeakyReLU denotes the activation function and GroupNorm normalizes feature channels to improve training stability and convergence.

The resulting multi-scale embeddings $\mathcal{H} = \{\mathbf{H}_0, \mathbf{H}_1, \mathbf{H}_2, \dots, \mathbf{H}_M\}$, where $\mathbf{H}_0 \in \mathbb{R}^{T \times \frac{H}{2^0} \times \frac{W}{2^0} \times D}$ retains fine-grained local representations and $\mathbf{H}_M \in \mathbb{R}^{T \times \frac{H}{2^M} \times \frac{W}{2^M} \times D}$ encodes coarse-scale global structures, capture multi-scale spatio-temporal features. These embeddings are then fed into the *Scale-bridging Spatio-Temporal Encoder*.

4.2 SCALE-BRIDGING SPATIO-TEMPORAL ENCODER

After obtaining the multi-scale Earth representations, we design a scale-bridging spatio-temporal encoder to jointly capture spatial dependencies, temporal dynamics, and inter-scale interactions. Unlike traditional meteorological models that often emphasize either temporal or spatial aspects in isolation, our encoder integrates both perspectives while enabling information flow across scales, which is critical for representing hierarchical atmospheric processes.

Spatial encoding. Given multi-scale features \mathcal{H} , each level is first processed by an independent spatial encoder inspired by the Vision Transformer (Dosovitskiy et al.) structure. Specifically, for the m -th scale and the n -th encoder layer, we perform 2D patch embedding, followed by multi-head self-attention and feed-forward transformations:

$$\mathbf{H}_m^{s'(n)} = \text{LayerNorm}(\text{Patch2D}(\mathbf{H}_m^{(n)})) + \text{MHA}(\text{LayerNorm}(\text{Patch2D}(\mathbf{H}_m^{(n)}))), \quad (2)$$

$$\mathbf{H}_m^{s(n)} = \text{DePatch2D}(\text{LayerNorm}(\mathbf{H}_m^{s'(n)}) + \text{FFN}(\text{LayerNorm}(\mathbf{H}_m^{s'(n)}))), \quad (3)$$

where Patch2D partitions the grid of size $\frac{H}{2^m} \times \frac{W}{2^m}$ into (P_1, P_2) patches, producing $\frac{H \times W}{P_1 \times P_2}$ tokens, and DePatch2D restores the tokenized representation back to its grid structure. This operation yields the spatial encoding $\mathbf{H}_m^{s(n)} \in \mathbb{R}^{T \times \frac{H}{2^m} \times \frac{W}{2^m} \times D}$, which captures scale-specific meteorological spatial dependencies.

Cross-scale message passing. To enhance coherence between adjacent scales, we introduce a cross-scale messaging mechanism. Information from the finer resolution is downsampled and injected into the coarser scale, facilitating hierarchical knowledge transfer:

$$\mathbf{H}_m^{c(n)} = \text{CrossScaleMessaging}(\mathbf{H}_{m-1}^{s(n)}) + \mathbf{H}_m^{s(n)}. \quad (4)$$

Here, CrossScaleMessaging is implemented as a stride-2 convolution, which aligns the resolution of $\mathbf{H}_{m-1}^{s(n)}$ with $\mathbf{H}_m^{s(n)}$. This design enables the encoder to integrate localized fine-grained patterns into broader global representations, crucial for multi-scale weather forecasting.

Temporal encoding. Finally, we model the temporal evolution of the cross-scale features $\mathbf{H}_m^{c(n)}$. While self-attention could be applied across temporal tokens, the extremely high dimensionality of meteorological grids makes it computationally prohibitive. Motivated by recent findings in long-term time series forecasting, we adopt a lightweight linear temporal encoder that achieves stable temporal modeling with minimal overhead:

$$\mathbf{H}_m^{t(n)} = W_2 \times \text{GELU}(W_1 \times \mathbf{H}_m^{s(n)} + B_1) + B_2 \quad (5)$$

This lightweight network is used to extract temporal dependencies. Here, $W_1 \in \mathbb{R}^{T \times 2T}$ and $W_2 \in \mathbb{R}^{T \times 2T}$, enabling effective modeling of historical time steps across multiple scales with an extremely small number of parameters (fewer than 100). It efficiently captures multi-scale temporal relationships in past observations.

4.3 LEVEL-ALIGNED FORECASTING DECODER

The outputs from the N -layer scale-bridging spatio-temporal encoder are subsequently fed into a level-aligned forecasting decoder to generate multi-scale forecasts of future atmospheric states. The decoder is designed to progressively reconstruct high-resolution spatio-temporal fields from the encoded representations, while ensuring that temporal forecasting and spatial upsampling remain coherent across scales. For each resolution level m , we apply an independent temporal linear layer that maps the T -step historical features into L -step future predictions. This design explicitly decouples temporal forecasting across scales, enabling each level to capture temporal dynamics consistent with its own resolution:

$$\mathbf{Z}_m = \text{Linear}_m(\mathbf{H}_m^{t(N)}) \in \mathbb{R}^{L \times \frac{H}{2^m} \times \frac{W}{2^m} \times D}. \quad (6)$$

To progressively upsample the spatial resolution, we adopt a depth-adaptive transposed convolution block. Each block doubles the resolution along both spatial dimensions, and the depth of upsampling is matched to the level index m . Thus, the m -th scale undergoes m successive upsampling layers, ensuring that coarse-scale features are refined consistently into finer spatial grids:

$$\mathbf{U}_m = \text{DeConv}^m(\mathbf{Z}_m) \in \mathbb{R}^{L \times H \times W \times D}. \quad (7)$$

This hierarchical upsampling ensures that global context encoded at coarse scales is gradually transformed into high-resolution local forecasts.

After spatial refinement, all scales share a common variable-wise linear projection layer, which maps the hidden dimension D into the full set of meteorological variables, including both surface and atmospheric fields. This shared mapping enforces consistency across scales and guarantees that all outputs lie in the same physical variable space:

$$\mathbf{V}_m = \text{Linear}_{var}(\mathbf{U}_m) \in \mathbb{R}^{L \times H \times W \times C}. \quad (8)$$

Finally, the forecasts from all scales are integrated to form the unified prediction. Each level provides complementary information, with fine-scale forecasts capturing localized details and coarse-scale forecasts contributing global stability. In EarthMix, this integration is performed by directly summing the scale-specific representations:

$$\hat{\mathbf{X}} = \text{EarthMix}(\{\mathbf{V}_m\}_{m=1}^M) \in \mathbb{R}^{L \times H \times W \times C}. \quad (9)$$

This simple aggregation efficiently combines multi-scale information to produce the final high-resolution, multi-variable prediction.

5 EXPERIMENTS

Dataset. We conduct experiments on the fifth generation of ECMWF Reanalysis data (ERA5) (Rasp et al., 2023). The temporal range spans from 1993 to 2021, where 1993–2017 is used for training, 2018–2019 for validation, and 2020–2021 for testing. We consider both atmospheric and surface variables. The atmospheric variables include five pressure-level quantities, each with 13 pressure levels: geopotential (Z), specific humidity (Q), temperature (T), and the U and V components of wind speed. The surface variables include 10-meter wind components (U10M, V10M), 2-meter temperature (T2M), total precipitation, and mean sea-level pressure (MSLP). To comprehensively evaluate our method, we construct three datasets at different spatial scales: **① Global-level:** We use the preprocessed ERA5 dataset with a 5.625° spatial resolution and 6-hour temporal frequency. **② Continental-level:** We extract ERA5 data over South America, covering the region from 56°S to 14°N and 81°W to 34°W , with a 1° spatial resolution. **③ Regional-level:** We extract a subset with 0.25° resolution over East Asia (20°N – 28°N , 110°E – 126°E). More data and pre-processing details are available in Appendix C

Metrics. To evaluate forecasting performance, we report two widely adopted metrics in numerical weather prediction: latitude-weighted Root Mean Squared Error (RMSE) and Anomaly Correlation Coefficient (ACC). All predictions are first de-normalized before metric computation. Given L forecasting steps, the prediction $\hat{x}_{\ell hw}$ and ground truth $y_{\ell hw}$ at lead time ℓ and spatial grid (h, w) , the metrics are defined as

$$\text{RMSE} = \frac{1}{L} \sum_{\ell=1}^L \sqrt{\frac{1}{HW} \sum_{h=1}^H \sum_{w=1}^W \alpha(h) (y_{\ell hw} - \hat{x}_{\ell hw})^2}, \text{ACC} = \frac{\sum_{\ell, h, w} \alpha(h) \tilde{y}_{\ell hw} \tilde{x}_{\ell hw}}{\sqrt{\sum_{\ell, h, w} \alpha(h) \tilde{y}_{\ell hw}^2} \sqrt{\sum_{\ell, h, w} \alpha(h) \tilde{x}_{\ell hw}^2}}, \quad (10)$$

where the latitude-dependent weight is $\alpha(h) = \cos(h) / \frac{1}{H} \sum_{h'=1}^H \cos(h')$, and $\tilde{y} = y - C$, $\tilde{x} = \hat{x} - C$ are anomalies relative to the empirical climatology $C = \frac{1}{LHW} \sum_{\ell, h, w} y_{\ell hw}$. More Details is in Appendix D.

Baselines. We benchmark our approach against a diverse set of representative baselines spanning operational weather forecasting models, spatio-temporal sequence learners, and image-based architectures. For single-step meteorological forecasting, we include **Pangu-Weather** (Bi et al., 2023), **FuXi** (Chen et al., 2023b), **FourCastNet (FCN)** (Pathak et al., 2022), and **Triton** (Wu et al., 2025a), which represent state-of-the-art Transformer-based designs for data-driven numerical weather prediction. For multi-step spatio-temporal modeling, we evaluate against **SimVP** (Gao et al., 2022a), a leading video prediction framework adapted for geophysical data. Additionally, we incorporate a canonical vision backbone, **U-Net** (Ronneberger et al., 2015), to assess the performance of convolutional architectures in this setting. All baselines are re-trained on our datasets with identical variables and splits to ensure fairness of comparison. More Details can be found in Appendix E.

5.1 GLOBAL WEATHER FORECASTING

Table 1: Quantitative comparison of short-term (up to 24 hours) global weather forecasting performance. Metrics are reported as weighted RMSE and ACC, averaged over $\Delta t = \{6, 12, 18, 24\}$ hours.

Metric	RMSE↓							ACC↑						
	Variable	STORM	Triton	Pangu	FCN	FuXi	SimVP	UNet	STORM	Triton	Pangu	FCN	FuXi	SimVP
T2M	0.675	0.873	1.106	1.579	1.356	1.343	2.445	0.999	0.998	0.997	0.994	0.995	0.996	0.986
U10	0.669	0.819	1.377	1.529	1.314	1.448	1.971	0.991	0.987	0.959	0.953	0.965	0.959	0.952
V10	0.713	0.868	1.483	1.658	1.381	1.556	1.867	0.984	0.976	0.924	0.910	0.940	0.923	0.915
Prec	5.4E-04	6.4E-04	8.4E-04	9.8E-04	8.7E-04	9.6E-04	1.0E-03	0.923	0.891	0.802	0.728	0.791	0.744	0.765
MSLP	71.8	93.7	215.8	217.1	170.1	185.8	257.5	0.998	0.996	0.978	0.979	0.988	0.986	0.976
U500	1.903	2.500	3.410	4.607	3.962	4.066	4.677	0.993	0.988	0.975	0.958	0.969	0.968	0.963
V500	2.055	2.597	3.709	5.021	4.160	4.380	4.999	0.983	0.974	0.942	0.899	0.934	0.926	0.914
T500	0.524	0.696	0.886	1.251	1.111	1.242	1.237	0.998	0.997	0.995	0.991	0.993	0.991	0.991
Z500	79.8	109.4	225.7	268.5	215.3	223.5	308.3	1.000	1.000	0.998	0.998	0.999	0.999	0.997
Q500	3.9E-05	5.0E-05	5.6E-05	7.3E-05	6.9E-05	7.7E-05	7.3E-05	0.976	0.962	0.949	0.918	0.926	0.909	0.924

Short-term Forecasting. We first evaluate the proposed multi-scale spatiotemporal forecasting model, STORM, on short-term global weather prediction. Specifically, we conduct 24-hour forecasts and compare our method against a range of state-of-the-art approaches, including Pangu, Fuxi, FourCastNet, Triton, SimVP, and U-Net. The evaluation covers both surface variables (2m temperature (T2M), 10m winds (U10, V10), precipitation (PREC), and mean sea level pressure (MSLP)) as well as mid-tropospheric fields (500 hPa U/V winds, temperature (T), geopotential height (Z), and specific humidity (Q)). For each method, we report weighted RMSE and ACC averaged over the prediction horizons $\Delta t = \{6, 12, 18, 24\}$ hours. The results, summarized in Table 1, show that STORM consistently achieves the best performance across all variables. In terms of RMSE, our method surpasses even Triton, a model particularly tailored for short-term forecasting, by a significant margin, while also delivering superior ACC scores. These improvements highlight the advantage of incorporating multi-scale spatiotemporal representations, which enable the model to capture both local details and global circulation patterns effectively. Full results are available at Appendix J.

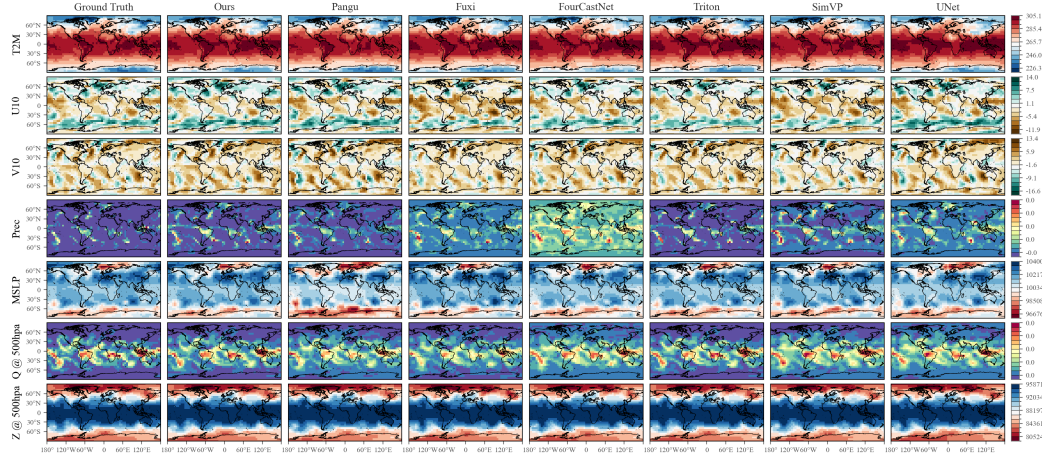


Figure 3: Visualization of 24-hour forecasts for multiple atmospheric variables.

To further illustrate the predictive capability of our model, Figure 3 visualizes 24-hour forecasts across multiple variables. Compared with other baselines, the predictions of STORM are visually closer to the ground-truth reanalysis, preserving fine-grained regional structures while maintaining coherent large-scale dynamics. These results confirm that our approach not only improves numerical accuracy but also produces more realistic spatial patterns in short-term global weather forecasting. The visualizations for all variables are provided in Appendix I.

Table 2: Quantitative comparison of long-term (7–10 days) global weather forecasting performance. Metrics are reported as weighted RMSE and ACC, averaged over $\Delta t = \{168, 192, 216, 240\}$ hours.

Metric	RMSE↓							ACC↑						
	Variable	STORM	Triton	Pangu	FCN	Fuxi	SimVP	UNet	STORM	Triton	Pangu	FCN	Fuxi	SimVP
T2M	2.596	3.386	3.633	4.181	3.500	3.168	4.477	0.984	0.965	0.955	0.971	0.969	0.976	0.937
U10	3.857	4.271	5.127	5.363	4.696	3.901	5.828	0.716	0.650	0.615	0.604	0.574	0.684	0.559
V10	4.106	4.504	5.095	5.569	4.795	4.180	6.045	0.464	0.370	0.325	0.297	0.282	0.383	0.262
Prec	1.4E-03	2.1E-03	1.8E-03	1.6E-03	1.6E-03	1.5E-03	2.3E-03	0.432	0.305	0.288	0.223	0.243	0.382	0.204
MSLP	735.4	815.6	1125.4	1041.4	950.0	784.7	1149.3	0.782	0.725	0.741	0.718	0.641	0.741	0.679
U925	6.582	8.918	10.794	9.159	10.152	8.117	12.236	0.884	0.787	0.803	0.793	0.747	0.827	0.747
V925	6.588	7.910	9.707	9.618	8.794	7.148	10.858	0.519	0.369	0.299	0.284	0.212	0.336	0.205
T925	2.797	3.718	4.308	3.879	4.513	3.565	5.331	0.966	0.937	0.931	0.938	0.912	0.945	0.902
Q925	3.3E-07	5.4E-07	4.5E-07	4.7E-07	5.5E-07	4.0E-07	6.3E-07	0.749	0.556	0.556	0.572	0.535	0.630	0.519
Z925	813.4	1049.4	1419.2	968.8	1304.1	1097.4	1537.9	0.981	0.959	0.955	0.963	0.958	0.971	0.936

Long-term Forecasting. Beyond short horizons, we further evaluate STORM on extended-range forecasting, covering 7-day, 8-day, 9-day, and 10-day predictions. Table 2 reports the average weighted RMSE and ACC across these horizons. The results show that STORM consistently outperforms all competing methods, with clear margins over strong baselines such as Pangu and

FourCastNet. Even at day 10, where the forecasting task becomes extremely challenging due to error accumulation and chaotic dynamics, our model maintains significantly lower RMSE and higher ACC, demonstrating its robustness and superior long-term predictive capability. Full results are available at Appendix K. To provide further insight, Figure 4 visualizes the evolution of RMSE and ACC from

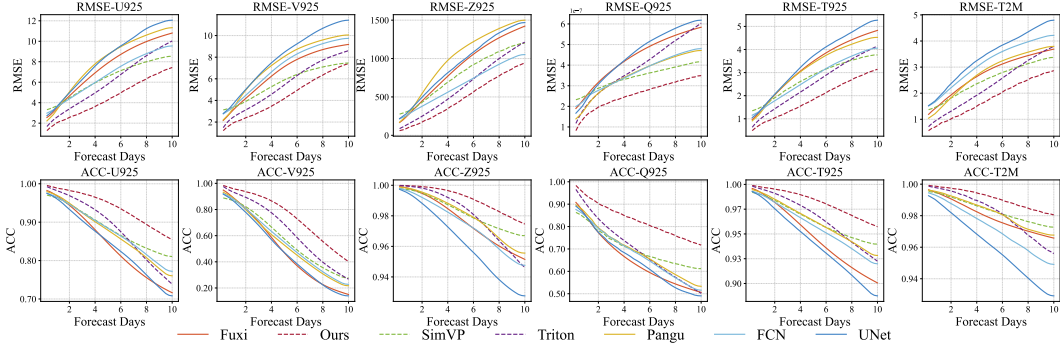


Figure 4: RMSE and ACC of U925, V925, Z925, Q925, T925, and T2M from day 1 to day 10.

day 1 to day 10 for several key variables, including U925, V925, Z925, Q925, T925, and T2M. We observe that different baseline methods tend to exhibit strengths over specific forecast horizons—for example, some achieve relatively competitive results at shorter lead times but deteriorate rapidly afterwards. In contrast, STORM consistently maintains the best accuracy across both short- and long-term horizons. This highlights the effectiveness of our multi-scale spatiotemporal design, which enables stable and reliable forecasts over a wide range of temporal scales.

5.2 REGIONAL HIGH RESOLUTION FORECASTING

To further demonstrate the scalability and robustness of our approach, we conduct forecasting experiments on higher-resolution regional subsets. Specifically, we consider two representative cases: Continental-level: South America, spanning from 56°S to 14°N and 81°W to 34°W, at 1° resolution; Regional-level: East Asia, spanning 20°N–28°N and 110°E–126°E, at 0.25° resolution. Table 3 summarizes the RMSE and ACC across all variables for horizons of 6 hours, 1 day, 4 days, 7 days, and 10 days. We observe that STORM consistently achieves the lowest RMSE and the highest ACC at both continental and regional scales, highlighting its ability to maintain strong predictive skill under different spatial resolutions. In particular, the advantage of STORM becomes more pronounced at longer horizons, demonstrating its superiority in long-range regional forecasting. Figure 5 provides a qualitative visualization of the 10-day forecasts for selected variables in both South America and East Asia. By zooming into local details, we see that STORM captures fine-grained structures more faithfully and is visually closer to the ground truth compared to baselines. These results confirm the effectiveness of our multi-scale design in enhancing both large-scale consistency and small-scale detail preservation.

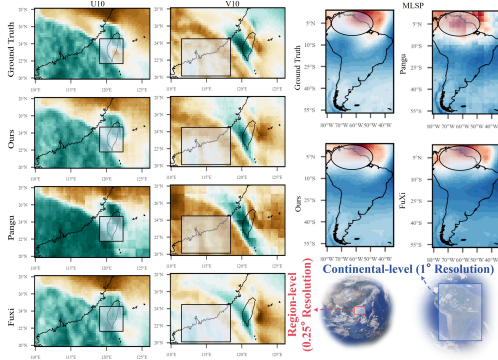


Figure 5: Visualization of 10-day forecasts over South America (1°) and East Asia (0.25°).

5.3 ABLATION STUDY

To better understand the contribution of each component in STORM, we conduct an ablation study by removing or modifying key modules. Specifically, we consider the following variants, ❶ **w/o T**: which removes the temporal evolution encoder from the encoder; ❷ **w/o M**: which changes the Hierarchical Earth Embedder, the Scale-Bridging Spatio-Temporal Encoder, and the Level-Aligned Forecasting Decoder to replace multi-scale modeling with single-scale modeling; ❸ **w/o S**: which removes the spatial encoder from the encoder.

Table 3: Regional high-resolution forecasting results. We report averaged results for 6 hours, 1 day, 4 days, 7 days, and 10 days over South America (1° resolution) and East Asia (0.25° resolution).

Data	Methods	6Hour		1Day		4Day		7Day		10Day	
		RMSE↓	ACC↑								
Cont-SA (1°)	STORM	0.874	0.945	1.560	0.847	2.866	0.601	3.322	0.519	3.510	0.499
	Triton	0.927	0.941	1.808	0.817	3.689	0.480	4.687	0.347	5.433	0.251
	FCN	1.411	0.933	2.466	0.816	4.186	0.498	5.176	0.425	6.018	0.403
	Pangu	0.989	0.876	1.794	0.702	3.557	0.440	4.235	0.375	4.613	0.368
	Fuxi	0.913	0.941	1.677	0.830	3.253	0.547	3.632	0.500	3.797	0.466
	SimVP	0.947	0.939	1.619	0.843	3.110	0.554	3.603	0.476	3.891	0.426
	UNet	1.528	0.873	2.696	0.661	6.994	0.291	11.50	0.248	15.62	0.252
Reg-EA (0.25°)	STORM	14.53	0.980	41.71	0.920	154.6	0.627	187.8	0.548	200.9	0.524
	Triton	14.55	0.976	51.65	0.919	183.7	0.579	218.7	0.499	234.3	0.482
	FCN	33.00	0.954	98.15	0.832	256.4	0.559	297.4	0.495	315.6	0.471
	Pangu	17.35	0.963	47.31	0.895	157.5	0.625	206.2	0.543	227.5	0.511
	Fuxi	17.69	0.969	54.67	0.903	178.1	0.592	211.2	0.522	227.7	0.493
	SimVP	32.17	0.935	53.44	0.887	158.5	0.615	189.0	0.546	202.5	0.523
	UNet	22.77	0.956	63.05	0.875	195.1	0.566	241.6	0.480	261.8	0.450

Figure 6 reports the RMSE for ten key variables: T2M, U10, V10, PREC, MSLP, U500, V500, T500, Q500, and Z500. The results demonstrate several important findings: (1) Every module contributes significantly to the overall forecasting performance; (2) The spatial encoder (S) plays a particularly critical role in improving prediction accuracy; (3) The combination of multi-scale mixing and spatial encoding achieves the largest performance gains, indicating that capturing both spatial dependencies and multi-scale interactions is crucial for accurate global weather forecasting. These observations confirm the effectiveness of our design in modeling complex spatiotemporal dependencies inherent in meteorological data.

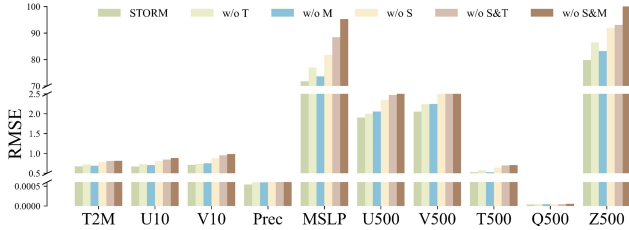


Figure 6: Ablation study results of STORM.

5.4 STORM ANALYSIS

We perform a multi-scale analysis of STORM to understand the contribution of different spatial scales to forecasting accuracy. Figure 7(a) visualizes predictions at different scales. The finest scale (scale0) captures rich local details, while the coarsest scale (scale2) better represents global circulation patterns. Individually, each scale exhibits distinct prediction errors, but combining multi-scale predictions results in the most accurate forecasts, demonstrating the effectiveness of multi-scale integration. Figure 7(b) further analyzes the effect of the number of scales as a hyperparameter. As the number of scales increases, the predictive performance improves, but the gains diminish beyond three scales. Based on this analysis, we set the number of scales in STORM to three, achieving a balance between local detail preservation and global structure representation.

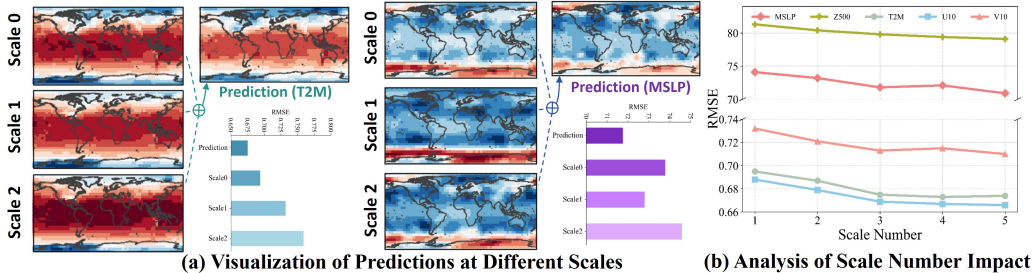


Figure 7: Visualization of multi-scale predictions and the analysis of scale number.

6 CONCLUSION

Despite rapid advances in deep learning for weather prediction, modeling atmospheric dynamics remains challenging due to their heterogeneous spatio-temporal scales. We introduced **STORM**, a unified framework with a Hierarchical Earth Embedder, a Scale-Bridging Spatio-Temporal Encoder, and a Level-Aligned Forecasting Decoder to explicitly capture cross-scale dependencies. Extensive experiments on ERA datasets with resolutions of 5.625° , 1° , and 0.25° show that **STORM** consistently achieves state-of-the-art performance across global and regional settings, as well as short- and long-term horizons. Our results highlight the necessity of synergistic multi-scale modeling for reliable weather forecasting. Looking ahead, we envision **STORM** as a step toward a new generation of spatio-temporal models that integrate fine-grained detail with global coherence, offering a foundation for more accurate, efficient, and robust climate and Earth system prediction.

ETHICS STATEMENT

All authors confirm compliance with the ICLR Code of Ethics. This study does not utilize human participants, private information, or sensitive content. Our work relies entirely on publicly available datasets and established benchmarks, with no anticipated negative social or environmental consequences. There are no conflicts of interest or external funding sources that might influence the findings.

REPRODUCIBILITY STATEMENT

We have taken care to ensure that our experiments can be replicated. The architecture and training details of our model are fully described in Sections 4 and Appendix E. All datasets are publicly accessible, and the preprocessing steps are documented in Appendix C. Furthermore, we provide anonymized code and usage instructions as supplementary material to support reproducibility of our results.

ACKNOWLEDGMENT

This paper is partially supported by the National Natural Science Foundation of China (No.62502488, No.12227901), Natural Science Foundation of Jiangsu Province (BK20240460), the grant from State Key Laboratory of Resources and Environmental Information System. The AI-driven experiments, simulations and model training were performed on the robotic AI-Scientist platform of Chinese Academy of Sciences.

REFERENCES

- Ulrich Achatz, M Joan Alexander, Erich Becker, Hye-Yeong Chun, Andreas Dörnbrack, Laura Holt, Riwal Plougonven, Inna Polichtchouk, Kaoru Sato, Aditi Sheshadri, et al. Atmospheric gravity waves: Processes and parameterization. *Journal of the Atmospheric Sciences*, 81(2):237–262, 2024.
- Santhosh Baboo and Kadar Shereef. An efficient weather forecasting system using artificial neural network. *International journal of environmental science and development*, 1(4):321, 2010.
- Peter Bauer, Alan Thorpe, and Gilbert Brunet. The quiet revolution of numerical weather prediction. *Nature*, 525(7567):47–55, 2015.
- Kaifeng Bi, Lingxi Xie, Hengheng Zhang, Xin Chen, Xiaotao Gu, and Qi Tian. Accurate medium-range global weather forecasting with 3d neural networks. *Nature*, 619:533–538, 2023.
- Michele Buzziotti, Benjamin A Storer, Hemant Khatri, Stephen M Griffies, and Hussein Aluie. Spatio-temporal coarse-graining decomposition of the global ocean geostrophic kinetic energy. *Journal of Advances in Modeling Earth Systems*, 15(6):e2023MS003693, 2023.

- Kang Chen, Tao Han, Junchao Gong, Lei Bai, Fenghua Ling, Jing-Jia Luo, Xi Chen, Leiming Ma, Tianning Zhang, Rui Su, et al. Fengwu: Pushing the skillful global medium-range weather forecast beyond 10 days lead. *arXiv preprint arXiv:2304.02948*, 2023a.
- Lei Chen, Xiaohui Zhong, Feng Zhang, Yuan Cheng, Yinghui Xu, Yuan Qi, and Hao Li. Fuxi: a cascade machine learning forecasting system for 15-day global weather forecast. *npj climate and atmospheric science*, 6(1):190, 2023b.
- Alexey Dosovitskiy, Lucas Beyer, Alexander Kolesnikov, Dirk Weissenborn, Xiaohua Zhai, Thomas Unterthiner, Mostafa Dehghani, Matthias Minderer, Georg Heigold, Sylvain Gelly, et al. An image is worth 16x16 words: Transformers for image recognition at scale. In *International Conference on Learning Representations*.
- Yuan Gao, Hao Wu, Ruiqi Shu, Huanshuo Dong, Fan Xu, Rui Chen, Yibo Yan, Qingsong Wen, Xuming Hu, Kun Wang, et al. Oneforecast: A universal framework for global and regional weather forecasting. *arXiv preprint arXiv:2502.00338*, 2025.
- Zhangyang Gao, Cheng Tan, Lirong Wu, and Stan Z Li. Simvp: Simpler yet better video prediction. In *Proceedings of the IEEE/CVF conference on computer vision and pattern recognition*, pp. 3170–3180, 2022a.
- Zhihan Gao, Xingjian Shi, Hao Wang, Yi Zhu, Yuyang Bernie Wang, Mu Li, and Dit-Yan Yeung. Earthformer: Exploring space-time transformers for earth system forecasting. *Advances in Neural Information Processing Systems*, 35:25390–25403, 2022b.
- Shengnan Guo, Youfang Lin, Huaiyu Wan, Xiucheng Li, and Gao Cong. Learning dynamics and heterogeneity of spatial-temporal graph data for traffic forecasting. *IEEE Transactions on Knowledge and Data Engineering*, 34(11):5415–5428, 2022. doi: 10.1109/TKDE.2021.3056502.
- Yifan Hu, Yuante Li, Peiyuan Liu, Yuxia Zhu, Naiqi Li, Tao Dai, Shu-tao Xia, Dawei Cheng, and Changjun Jiang. Fintsb: A comprehensive and practical benchmark for financial time series forecasting. *arXiv preprint arXiv:2502.18834*, 2025a.
- Yifan Hu, Peiyuan Liu, Peng Zhu, Dawei Cheng, and Tao Dai. Adaptive multi-scale decomposition framework for time series forecasting. In *Proceedings of the AAAI Conference on Artificial Intelligence*, volume 39, pp. 17359–17367, 2025b.
- Yifan Hu, Jie Yang, Tian Zhou, Peiyuan Liu, Yujin Tang, Rong Jin, and Liang Sun. Bridging past and future: Distribution-aware alignment for time series forecasting. In *The Fourteenth International Conference on Learning Representations*, 2026.
- Qihe Huang, Lei Shen, Ruixin Zhang, Jiahuan Cheng, Shouhong Ding, Zhengyang Zhou, and Yang Wang. Hdmixer: Hierarchical dependency with extendable patch for multivariate time series forecasting. In *Proceedings of the AAAI Conference on Artificial Intelligence*, volume 38, pp. 12608–12616, 2024a.
- Qihe Huang, Lei Shen, Ruixin Zhang, Shouhong Ding, Binwu Wang, Zhengyang Zhou, and Yang Wang. Crossgnn: Confronting noisy multivariate time series via cross interaction refinement. *Advances in Neural Information Processing Systems*, 36, 2024b.
- Qihe Huang, Zhengyang Zhou, Kuo Yang, Gengyu Lin, Zhongchao Yi, and Yang Wang. Leret: Language-empowered retentive network for time series forecasting. In Kate Larson (ed.), *Proceedings of the Thirty-Third International Joint Conference on Artificial Intelligence, IJCAI-24*, pp. 4165–4173. International Joint Conferences on Artificial Intelligence Organization, 8 2024c. doi: 10.24963/ijcai.2024/460. URL <https://doi.org/10.24963/ijcai.2024/460>. Main Track.
- Qihe Huang, Zhengyang Zhou, Yangze Li, Kuo Yang, Binwu Wang, and Yang Wang. Many minds, one goal: Time series forecasting via sub-task specialization and inter-agent cooperation. In *The Thirty-ninth Annual Conference on Neural Information Processing Systems*, 2025a.

- Qihe Huang, Zhengyang Zhou, Kuo Yang, and Yang Wang. Exploiting language power for time series forecasting with exogenous variables. In *Proceedings of the ACM on Web Conference 2025, WWW '25*, pp. 4043–4052, New York, NY, USA, 2025b. Association for Computing Machinery. ISBN 9798400712746. doi: 10.1145/3696410.3714793. URL <https://doi.org/10.1145/3696410.3714793>.
- Qihe Huang, Zhengyang Zhou, Kuo Yang, Zhongchao Yi, Xu Wang, and Yang Wang. Timebase: The power of minimalism in efficient long-term time series forecasting. In *Forty-second International Conference on Machine Learning, 2025c*.
- Diederik P Kingma. Adam: A method for stochastic optimization. *arXiv preprint arXiv:1412.6980*, 2014.
- Robert Kuligowski and Ana Barros. Localized precipitation forecasts from a numerical weather prediction model using artificial neural networks. *Weather and forecasting*, 13(4):1194–1204, 1998.
- Remi Lam, Alvaro Sanchez-Gonzalez, Matthew Willson, Peter Wirsberger, Meire Fortunato, Alexander Pritzel, Suman Ravuri, Timo Ewalds, Ferran Alet, Zach Eaton-Rosen, et al. GraphCast: Learning skillful medium-range global weather forecasting. *arXiv*, 2022.
- Zhengyu Li, Xiangfei Qiu, Yuhan Zhu, Xingjian Wu, Jilin Hu, Chenjuan Guo, and Bin Yang. Gcgnet: Graph-consistent generative network for time series forecasting with exogenous variables. In *ICLR*, 2026.
- Yuxuan Liang, Haomin Wen, Yutong Xia, Ming Jin, Bin Yang, Flora Salim, Qingsong Wen, Shirui Pan, and Gao Cong. Foundation models for spatio-temporal data science: A tutorial and survey. In *Proceedings of the 31st ACM SIGKDD Conference on Knowledge Discovery and Data Mining V. 2*, pp. 6063–6073, 2025.
- Shengsheng Lin, Weiwei Lin, Wentai Wu, Feiyu Zhao, Ruichao Mo, and Haotong Zhang. Seg-rnn: Segment recurrent neural network for long-term time series forecasting. *arXiv preprint arXiv:2308.11200*, 2023.
- Xvyuan Liu, Xiangfei Qiu, Hanyin Cheng, Xingjian Wu, Chenjuan Guo, Bin Yang, and Jilin Hu. Astgi: Adaptive spatio-temporal graph interactions for irregular multivariate time series forecasting. In *ICLR*, 2026a.
- Xvyuan Liu, Xiangfei Qiu, Xingjian Wu, Zhengyu Li, Chenjuan Guo, Jilin Hu, and Bin Yang. Rethinking irregular time series forecasting: A simple yet effective baseline. In *AAAI*, 2026b.
- Jiaming Ma, Zhiqing Cui, Binwu Wang, Pengkun Wang, Zhengyang Zhou, Zhe Zhao, and Yang Wang. Causal learning meet covariates: Empowering lightweight and effective nationwide air quality forecasting. 2025a.
- Jiaming Ma, Binwu Wang, Qihe Huang, Guanjun Wang, Pengkun Wang, Zhengyang Zhou, and Yang Wang. Mofo: Empowering long-term time series forecasting with periodic pattern modeling. In *Advances in Neural Information Processing Systems*, 2025b.
- Jiaming Ma, Binwu Wang, Guanjun Wang, Kuo Yang, Zhengyang Zhou, Pengkun Wang, Xu Wang, and Yang Wang. Less but more: Linear adaptive graph learning empowering spatiotemporal forecasting. In *Advances in Neural Information Processing Systems*, 2025c.
- Jiaming Ma, Binwu Wang, Pengkun Wang, Zhengyang Zhou, Xu Wang, and Yang Wang. Bist: A lightweight and efficient bi-directional model for spatiotemporal prediction. *Proceedings of the VLDB Endowment*, 18(6):1663–1676, 2025d.
- Jiaming Ma, Binwu Wang, Pengkun Wang, Zhengyang Zhou, Xu Wang, and Yang Wang. Robust spatio-temporal centralized interaction for ood learning. In *Forty-second International Conference on Machine Learning, 2025e*.
- Jiaming Ma, Binwu Wang, Pengkun Wang, Zhengyang Zhou, Yudong Zhang, Xu Wang, and Yang Wang. Mobimixer: A multi-scale spatiotemporal mixing model for mobile traffic prediction. *IEEE Transactions on Mobile Computing*, 2025f.

- Jiaming Ma, Qihe Huang, Guanjun Wang, Haofeng Ma, Sheng Huang, Zhengyang Zhou, Pengkun Wang, Binwu Wang, and Yang Wang. Phat: Modeling period heterogeneity for multivariate time series forecasting. *The Fourteenth International Conference on Learning Representations*, 2026a.
- Jiaming Ma, Siyuan Mu, Ruilin Tang, Haofeng Ma, Qihe Huang, Zhengyang Zhou, Pengkun Wang, Binwu Wang, and Yang Wang. To see far, look close: Evolutionary forecasting for long-term time series. *arXiv preprint arXiv:2601.23114*, 2026b.
- Tung Nguyen, Johannes Brandstetter, Ashish Kapoor, Jayesh K Gupta, and Aditya Grover. ClimaX: A foundation model for weather and climate. In *ICML*, 2023.
- Adam Paszke, Sam Gross, Francisco Massa, Adam Lerer, James Bradbury, Gregory Chanan, Trevor Killeen, Zeming Lin, Natalia Gimelshein, Luca Antiga, et al. Pytorch: An imperative style, high-performance deep learning library. *Advances in neural information processing systems*, 32, 2019.
- Jaideep Pathak, Shashank Subramanian, Peter Harrington, Sanjeev Raja, Ashesh Chattopadhyay, Morteza Mardani, Thorsten Kurth, David Hall, Zongyi Li, Kamyar Azizzadenesheli, et al. FourCast-Net: A global data-driven high-resolution weather model using adaptive fourier neural operators. *arXiv*, 2022.
- Xiangfei Qiu, Jilin Hu, Lekui Zhou, Xingjian Wu, Junyang Du, Buang Zhang, Chenjuan Guo, Aoying Zhou, Christian S. Jensen, Zhenli Sheng, and Bin Yang. TFB: Towards comprehensive and fair benchmarking of time series forecasting methods. In *Proc. VLDB Endow.*, pp. 2363–2377, 2024.
- Xiangfei Qiu, Zhe Li, Wanghui Qiu, Shiyuan Hu, Lekui Zhou, Xingjian Wu, Zhengyu Li, Chenjuan Guo, Aoying Zhou, Zhenli Sheng, Jilin Hu, Christian S. Jensen, and Bin Yang. Tab: Unified benchmarking of time series anomaly detection methods. In *Proc. VLDB Endow.*, pp. 2775–2789, 2025a.
- Xiangfei Qiu, Xingjian Wu, Hanyin Cheng, Xuyuan Liu, Chenjuan Guo, Jilin Hu, and Bin Yang. Dbloss: Decomposition-based loss function for time series forecasting. In *NeurIPS*, 2025b.
- Xiangfei Qiu, Xingjian Wu, Yan Lin, Chenjuan Guo, Jilin Hu, and Bin Yang. DUET: Dual clustering enhanced multivariate time series forecasting. In *SIGKDD*, pp. 1185–1196, 2025c.
- Xiangfei Qiu, Yuhan Zhu, Zhengyu Li, Xingjian Wu, Bin Yang, and Jilin Hu. Dag: A dual correlation network for time series forecasting with exogenous variables. *arXiv preprint arXiv:2509.14933*, 2025d.
- Stephan Rasp, Stephan Hoyer, Alexander Merose, Ian Langmore, Peter Battaglia, Tyler Russel, Alvaro Sanchez-Gonzalez, Vivian Yang, Rob Carver, Shreya Agrawal, et al. Weatherbench 2: A benchmark for the next generation of data-driven global weather models. *arXiv preprint arXiv:2308.15560*, 2023.
- Olaf Ronneberger, Philipp Fischer, and Thomas Brox. U-net: Convolutional networks for biomedical image segmentation. In *Medical Image Computing and Computer-Assisted Intervention (MICCAI)*. Springer, 2015.
- Xingjian Shi, Zhourong Chen, Hao Wang, Dit-Yan Yeung, Wai-Kin Wong, and Wang-chun Woo. Convolutional lstm network: A machine learning approach for precipitation nowcasting. *Advances in neural information processing systems*, 28, 2015.
- Binwu Wang, Yudong Zhang, Xu Wang, Pengkun Wang, Zhengyang Zhou, Lei Bai, and Yang Wang. Pattern expansion and consolidation on evolving graphs for continual traffic prediction. In *Proceedings of the 29th ACM SIGKDD Conference on Knowledge Discovery and Data Mining*, pp. 2223–2232, 2023a.
- Binwu Wang, Pengkun Wang, Yudong Zhang, Xu Wang, Zhengyang Zhou, Lei Bai, and Yang Wang. Towards dynamic spatial-temporal graph learning: A decoupled perspective. In *Proceedings of the AAAI Conference on Artificial Intelligence*, volume 38, pp. 9089–9097, 2024a.

- Hao Wang, Zhiyu Wang, Yunlong Niu, Zhaoran Liu, Haozhe Li, Yilin Liao, Yuxin Huang, and Xinggao Liu. An accurate and interpretable framework for trustworthy process monitoring. *IEEE Transactions on Artificial Intelligence*, 5(5):2241–2252, 2023b.
- Hao Wang, Haoxuan Li, Xu Chen, Mingming Gong, Zhichao Chen, et al. Optimal transport for time series imputation. In *The Thirteenth International Conference on Learning Representations*, 2025a.
- Hao Wang, Lichen Pan, Yuan Shen, Zhichao Chen, Degui Yang, Yifei Yang, Sen Zhang, Xinggao Liu, Haoxuan Li, and Dacheng Tao. Fredf: Learning to forecast in the frequency domain. In *The Thirteenth International Conference on Learning Representations*, 2025b.
- Hao Wang, Licheng Pan, Zhichao Chen, Xu Chen, Qingyang Dai, Lei Wang, Haoxuan Li, and Zhouchen Lin. Time-o1: Time-series forecasting needs transformed label alignment. 2025c.
- Hao Wang, Zhichao Che, Licheng Pan, Xiaoyu Jiang, Yichen Song, Qunshan He, and Xinggao Li. Deepfilter: A transformer-style framework for accurate and efficient process monitoring. *IEEE Transactions on Artificial Intelligence*, pp. 1–13, 2026a.
- Hao Wang, Licheng Pan, Yuan Lu, Zhichao Chen, Tianqiao Liu, Shuting He, Zhixuan Chu, Qingsong Wen, Haoxuan Li, and Zhouchen Lin. Quadratic direct forecast for training multi-step time-series forecast models. In *ICLR*, pp. 1–9, 2026b.
- Hao Wang, Licheng Pan, Yuan Lu, Zhixuan Chu, Xiaoxi Li, Shuting He, Zhichao Chen, Haoxuan Li, Qingsong Wen, and Zhouchen Lin. Distdf: Time-series forecasting needs joint-distribution wasserstein alignment. In *ICLR*, pp. 1–9, 2026c.
- Shiyu Wang, Haixu Wu, Xiaoming Shi, Tengge Hu, Huakun Luo, Lintao Ma, James Y Zhang, and JUN ZHOU. Timemixer: Decomposable multiscale mixing for time series forecasting. In *The Twelfth International Conference on Learning Representations*, 2024b.
- Yunbo Wang, Mingsheng Long, Jianmin Wang, Zhifeng Gao, and Philip S Yu. PredRNN: Recurrent neural networks for predictive learning using spatiotemporal LSTMs. In *Advances in Neural Information Processing Systems*, pp. 879–888, 2017.
- Jonathan Weyn, Dale Durrant, Rich Caruana, and Nathaniel Cresswell-Clay. Sub-seasonal forecasting with a large ensemble of deep-learning weather prediction models. *Journal of Advances in Modeling Earth Systems*, 13(7), 2021.
- Hao Wu, Yuan Gao, Ruiqi Shu, Kun Wang, Ruijian Gou, Chuhan Wu, Xinliang Liu, Juncai He, Shuhao Cao, Junfeng Fang, Xingjian Shi, Feng Tao, Qi Song, Shengxuan Ji, Yanfei Xiang, Yuze Sun, Jiahao Li, Fan Xu, Huanshuo Dong, Haixin Wang, Fan Zhang, Penghao Zhao, Xian Wu, Qingsong Wen, Deliang Chen, and Xiaomeng Huang. Advanced long-term earth system forecasting by learning the small-scale nature. *arXiv preprint arXiv:2505.19432*, 2025a.
- Xingjian Wu, Xiangfei Qiu, Hanyin Cheng, Zhengyu Li, Jilin Hu, Chenjuan Guo, and Bin Yang. Enhancing time series forecasting through selective representation spaces: A patch perspective. In *NeurIPS*, 2025b.
- Xingjian Wu, Xiangfei Qiu, Hongfan Gao, Jilin Hu, Bin Yang, and Chenjuan Guo. K²VAE: A koopman-kalman enhanced variational autoencoder for probabilistic time series forecasting. In *ICML*, 2025c.
- Xingjian Wu, Jianxin Jin, Wanghui Qiu, Peng Chen, Yang Shu, Bin Yang, and Chenjuan Guo. Aurora: Towards universal generative multimodal time series forecasting. In *ICLR*, 2026.
- Zonghan Wu, Shirui Pan, Guodong Long, Jing Jiang, and Chengqi Zhang. Graph wavenet for deep spatial-temporal graph modeling. *arXiv preprint arXiv:1906.00121*, 2019.
- Bing Yu, Haoteng Yin, and Zhanxing Zhu. Spatio-temporal graph convolutional networks: A deep learning framework for traffic forecasting. In *Proceedings of the 27th International Joint Conference on Artificial Intelligence (IJCAI)*, 2018.

Wenzhen Yue, Yong Liu, Hao Wang, Haoxuan Li, Xianghua Ying, Ruohao Guo, Bowei Xing, and Ji Shi. Olinear: A linear model for time series forecasting in orthogonally transformed domain. *Advances in Neural Information Processing Systems*, 2025.

Yudong Zhang, Binwu Wang, Ziyang Shan, Zhengyang Zhou, and Yang Wang. Cmt-net: A mutual transition aware framework for taxicab pick-ups and drop-offs co-prediction. In *Proceedings of the Fifteenth ACM International Conference on Web Search and Data Mining*, pp. 1406–1414, 2022.

Zhengyang Zhou, Qihe Huang, Gengyu Lin, Kuo Yang, LEI BAI, and Yang Wang. GReto: Remedying dynamic graph topology-task discordance via target homophily. In *The Eleventh International Conference on Learning Representations*, 2023. URL https://openreview.net/forum?id=8duT3mi_5n.

Appendix

Table of Contents

A	LLM Usage	17
B	Theoretical analysis: why multi-scale modeling helps	17
B.1	Setup and assumptions	17
B.2	Generalization bound improvement	17
B.3	Improved optimization speed regarding convergency	18
B.4	Putting pieces together: overall error and sample complexity	18
C	More Data Details	19
D	More Metric Details	20
E	More Implementation Details	20
F	Efficiency Analysis	20
G	Full Sensitive Analysis	21
H	More Details of Ablation Analysis	21
I	Forecast Visualization	22
I.1	Mean Sea Level Pressure (MSLP)	22
I.2	Specific Humidity at 500 hPa (Q500)	23
I.3	Precipitation	24
I.4	2-meter Temperature (T2M)	25
I.5	Temperature at 500 hPa (T500)	26
I.6	10-meter Zonal Wind (U10)	27
I.7	Zonal Wind at 500 hPa (U500)	28
I.8	10-meter Meridional Wind (V10)	29
I.9	Meridional Wind at 500 hPa (V500)	30
I.10	Geopotential Height at 500 hPa (Z500)	31
J	Full short-term forecasting results.	32
K	Full long-term forecasting results.	33

A LLM USAGE

Following the conference guidelines regarding large language models (LLMs), we disclose that LLMs were utilized solely to improve sentence clarity and grammatical correctness. All aspects of conceptual development, experimental methodology, data analysis, and core manuscript content were independently produced by the authors without LLM assistance

B THEORETICAL ANALYSIS: WHY MULTI-SCALE MODELING HELPS

In this section we present theoretical results that explain why a synergistic cross-scale spatio-temporal architecture can outperform a single-scale counterpart in (i) statistical generalization (smaller expected prediction error) and (ii) optimization speed (faster convergence). We adopt a bias–variance decomposition perspective for generalization, and a condition-number / PL-type argument for optimization. Proofs are sketched; full technical details follow the argument outlines below.

B.1 SETUP AND ASSUMPTIONS

Let $\mathbf{X} = \mathbb{R}^{T \times C \times H \times W}$ denote one time-slice grid and consider a target spatio-temporal mapping $f^* : \mathbb{R}^{T \times C \times H \times W} \rightarrow \mathbb{R}^{L \times C \times H \times W}$ that maps T historical frames to L future frames (all variables vectorized as needed). Denote by \mathcal{D} the data distribution and by $(\mathbf{X}_i, Y_i)_{i=1}^n \sim \mathcal{D}$ the training set. We consider two model classes: ① **Single-scale model** $\mathcal{F}_{\text{single}}$ of effective parameter-dimension d (e.g., a monolithic spatio-temporal network operating at full resolution). ② **Multi-scale model** \mathcal{F}_{ms} which decomposes the prediction into M scale-specific modules with parameter-dimensions d_1, \dots, d_M (so $\sum_{m=1}^M d_m = d$ or $\leq d$ depending on parameter sharing). We make standard regularity assumptions: **Assumption B.1** (Decomposability). *The target admits a scale decomposition*

$$f^* = \sum_{m=1}^M f_m^*, \quad f_m^* \in \mathcal{G}_m,$$

where each f_m^* captures variations at spatial scale m , and \mathcal{G}_m is the function space for scale m signals (e.g., fine, medium, or coarse patterns).

Assumption B.2 (Model capacity allocation). *Each scale-model class \mathcal{F}_m has Rademacher complexity $\mathfrak{R}_n(\mathcal{F}_m) \leq \rho_m \sqrt{\frac{d_m}{n}}$ for constants $\rho_m > 0$, while the single-scale class satisfies $\mathfrak{R}_n(\mathcal{F}_{\text{single}}) \leq \rho \sqrt{\frac{d}{n}}$.*

Assumption B.3 (PL condition for optimization). *The empirical loss $\hat{L}(\theta)$ is L -smooth and satisfies the Polyak–Lojasiewicz (PL) inequality in neighborhoods of interest: there exists $\mu > 0$ s.t.*

$$\frac{1}{2} \|\nabla \hat{L}(\theta)\|^2 \geq \mu (\hat{L}(\theta) - \hat{L}^*).$$

B.2 GENERALIZATION BOUND IMPROVEMENT

We first bound the excess risk (population loss minus Bayes risk) via a bias–variance decomposition and Rademacher complexity.

Theorem B.1 (Generalization bound improvement). *Assume squared loss and hypotheses above. Let \hat{f}_{single} and $\hat{f}_{\text{ms}} = \sum_{m=1}^M \hat{f}_m$ be ERM solutions in $\mathcal{F}_{\text{single}}$ and \mathcal{F}_{ms} respectively. Then with probability at least $1 - \delta$,*

$$\mathcal{E}(\hat{f}_{\text{single}}) \leq \underbrace{\inf_{f \in \mathcal{F}_{\text{single}}} \|f - f^*\|^2}_{\text{approx.}} + B \rho \sqrt{\frac{d}{n}} + O\left(\sqrt{\frac{\log(1/\delta)}{n}}\right),$$

and

$$\mathcal{E}(\hat{f}_{\text{ms}}) \leq \underbrace{\sum_{m=1}^M \inf_{g \in \mathcal{F}_m} \|g - f_m^*\|^2}_{\text{multi-scale approx.}} + B \sum_{m=1}^M \rho_m \sqrt{\frac{d_m}{n}} + O\left(\sqrt{\frac{\log(1/\delta)}{n}}\right),$$

where $B > 0$ is a universal constant and \mathcal{E} denotes population mean squared error.

Proof sketch. Standard decomposition: population risk = approximation error + estimation error. Estimation error is controlled by Rademacher complexity; using Assumption 2 we get the stated $\rho\sqrt{d/n}$ (single) and sum of $\rho_m\sqrt{d_m/n}$ (multi-scale). The remainder term follows from concentration (Talagrand / McDiarmid), yielding the $\sqrt{\log(1/\delta)/n}$ term. \square

Interpretation. If (i) the decomposition is faithful so that each f_m^* is well-approximated by \mathcal{F}_m (small multi-scale approximation error), and (ii) the per-scale capacities d_m concentrate (e.g. $d_m \ll d$), then

$$\sum_{m=1}^M \sqrt{d_m} \ll \sqrt{d},$$

hence the multi-scale estimation term $\sum_m \rho_m \sqrt{d_m/n}$ can be substantially smaller than $\rho\sqrt{d/n}$, yielding better generalization. Concretely, if $d_m \approx d/M$ and $\rho_m \approx \rho$, then

$$\sum_{m=1}^M \sqrt{d_m} = M \sqrt{\frac{d}{M}} = \sqrt{Md} < \sqrt{d} \quad \text{iff } M < 1,$$

so naive equal partition does not help; however, real atmospheric signals are *compressible*: coarse scales require tiny d_m and only few fine-scale components need larger d_m , making $\sum_m \sqrt{d_m} \ll \sqrt{d}$ in practice. Thus the bound formalizes a *bias-variance tradeoff* where multi-scale modeling reduces variance without materially increasing approximation bias.

B.3 IMPROVED OPTIMIZATION SPEED REGARDING CONVERGENCY

We now sketch how hierarchical (coarse-to-fine) architectures improve optimization by reducing effective condition numbers and enabling faster gradient-based convergence.

Theorem B.2 (Improved optimization speed regarding convergency). *Under Assumption 3 (PL inequality and L -smoothness) consider gradient descent with step size $\eta \leq 1/L$. Let $\kappa_{\text{single}} = L/\mu$ denote the condition number for the single-scale parameterization, and let κ_{ms} be the effective condition number for a multi-scale architecture that first fits coarse parameters and then refines fine parameters (blockwise parameterization). If the cross-scale coupling operator has spectral gap $\gamma \in (0, 1)$, then*

$$\kappa_{\text{ms}} \leq (1 - \gamma) \kappa_{\text{single}},$$

and gradient descent on \mathcal{F}_{ms} converges linearly as

$$\hat{L}(\theta_t) - \hat{L}^* \leq (1 - \eta\mu(1 - \gamma))^t (\hat{L}(\theta_0) - \hat{L}^*).$$

Proof sketch. Block-partition the parameter vector $\theta = [\theta_{\text{coarse}}, \theta_{\text{fine}}]$. The Hessian H of the empirical loss can be written in block form; coarse-to-fine structure makes the off-diagonal blocks small relative to diagonal blocks due to localization (this is the spectral gap γ). Using matrix perturbation bounds (Weyl-type inequalities) one shows the largest-to-smallest eigenvalue ratio of H is reduced by factor $(1 - \gamma)$. Under PL, GD attains linear rate with factor $1 - \eta\mu_{\text{eff}}$, where $\mu_{\text{eff}} = \mu(1 - \gamma)$. \square

Remarks. The spectral-gap condition formalizes the intuition that coarse-scale variables capture low-frequency, high-energy components and are weakly coupled to many fine-scale modes; explicit coarse-to-fine parametrization reduces ill-conditioning caused by high-frequency components and thus accelerates optimization.

B.4 PUTTING PIECES TOGETHER: OVERALL ERROR AND SAMPLE COMPLEXITY

Combining generalization and optimization insights yields a unified statement.

Corollary B.3 (Sample-complexity advantage). *Suppose the decomposition is faithful and the optimizer attains an ϵ -accurate empirical minimizer in $T(\epsilon)$ iterations (GD linear convergence as above). Then to achieve population error $\mathcal{E} \leq \epsilon$, the multi-scale model requires*

$$n_{\text{ms}} = \tilde{O}\left(\frac{1}{\epsilon^2} \left(\sum_{m=1}^M \rho_m \sqrt{d_m}\right)^2\right)$$

samples, while the single-scale model requires

$$n_{\text{single}} = \tilde{O}\left(\frac{1}{\epsilon^2} \rho^2 d\right).$$

If $\sum_m \sqrt{d_m} \ll \sqrt{d}$, then $n_{\text{ms}} \ll n_{\text{single}}$.

C MORE DATA DETAILS

To provide a more comprehensive description of the experimental setup, we summarize the datasets used in this work in Table 4. As introduced in the main text, all datasets are derived from the ERA5 reanalysis, covering the period from 1993 to 2021. Specifically, we split the data into 1993–2017 for training, 2018–2019 for validation, and 2020–2021 for testing. For atmospheric variables, we include five pressure-level quantities, geopotential (Z), specific humidity (Q), temperature (T), and the U and V components of wind, each defined on 13 standard pressure levels. For surface variables, we consider 10-meter wind components (U10M, V10M), 2-meter temperature (T2M), mean sea-level pressure (MSLP), and accumulated precipitation. Note that in Global- and Continental-level settings, precipitation is additionally included compared to the original 69 ERA5 variables, while in the Regional-level dataset only near-surface variables (T2M, U10M, V10M) are used. Regarding spatial coverage, we construct three datasets with different geographical ranges and resolutions: (i) **Global-level**: 5.625° resolution with 6-hour temporal frequency; (ii) **Continental-level**: 1° resolution over South America (56°S – 14°N , 81°W – 34°W); and (iii) **Regional-level**: 0.25° resolution over East Asia (20°N – 28°N , 110°E – 126°E). For preprocessing, we standardize each variable using statistics (mean and standard deviation) computed from the training set only. During inference, model predictions are rescaled back (de-normalized) to the original physical units to ensure consistency with evaluation metrics. This normalization scheme improves model stability and comparability across heterogeneous variables.

Table 4: The data details.

TASK	VARIABLE NAME	LAYERS	SPATIAL RESOLUTION	TEMPORAL FREQUENCY	LAT-LON RANGE
GLOBAL	GEOPOTENTIAL (Z)	13	5.625°	6H	-90°S – 90°N , 180°W – 180°E
	SPECIFIC HUMIDITY (Q)	13	5.625°	6H	-90°S – 90°N , 180°W – 180°E
	TEMPERATURE (T)	13	5.625°	6H	-90°S – 90°N , 180°W – 180°E
	U COMPONENT OF WIND (U)	13	5.625°	6H	-90°S – 90°N , 180°W – 180°E
	V COMPONENT OF WIND (V)	13	5.625°	6H	-90°S – 90°N , 180°W – 180°E
	10M U WIND (U10)	1	5.625°	6H	-90°S – 90°N , 180°W – 180°E
	10M V WIND (V10)	1	5.625°	6H	-90°S – 90°N , 180°W – 180°E
	2M TEMPERATURE (T2M)	1	5.625°	6H	-90°S – 90°N , 180°W – 180°E
	MEAN SEA LEVEL PRESSURE (MSLP)	1	5.625°	6H	-90°S – 90°N , 180°W – 180°E
	TOTAL PRECIPITATION (PREC)	1	5.625°	6H	-90°S – 90°N , 180°W – 180°E
CONTINENTAL	GEOPOTENTIAL (Z)	13	1.0°	6H	56°S – 14°N , 81°W – 34°W
	SPECIFIC HUMIDITY (Q)	13	1.0°	6H	SAME AS ABOVE
	TEMPERATURE (T)	13	1.0°	6H	SAME AS ABOVE
	U COMPONENT OF WIND (U)	13	1.0°	6H	SAME AS ABOVE
	V COMPONENT OF WIND (V)	13	1.0°	6H	SAME AS ABOVE
	10M U WIND (U10)	1	1.0°	6H	SAME AS ABOVE
	10M V WIND (V10)	1	1.0°	6H	SAME AS ABOVE
	2M TEMPERATURE (T2M)	1	1.0°	6H	SAME AS ABOVE
	MEAN SEA LEVEL PRESSURE (MSLP)	1	1.0°	6H	SAME AS ABOVE
	TOTAL PRECIPITATION (PREC)	1	1.0°	6H	SAME AS ABOVE
REGIONAL	2M TEMPERATURE (T2M)	1	0.25°	6H	20°N – 28°N , 110°E – 126°E
	10M U WIND (U10)	1	0.25°	6H	SAME AS ABOVE
	10M V WIND (V10)	1	0.25°	6H	SAME AS ABOVE

D MORE METRIC DETAILS

To evaluate forecasting skill, we follow standard practices in numerical weather prediction and report latitude-weighted Root Mean Squared Error (RMSE) and Anomaly Correlation Coefficient (ACC). Before computing the metrics, model outputs are de-normalized back to physical units for consistency with observations.

$$\text{RMSE} = \frac{1}{L} \sum_{\ell=1}^L \sqrt{\frac{1}{HW} \sum_{h=1}^H \sum_{w=1}^W \alpha(h) (y_{\ell hw} - \hat{x}_{\ell hw})^2}, \quad (11)$$

$$\text{ACC} = \frac{\sum_{\ell,h,w} \alpha(h) \tilde{y}_{\ell hw} \tilde{\hat{x}}_{\ell hw}}{\sqrt{\sum_{\ell,h,w} \alpha(h) \tilde{y}_{\ell hw}^2} \sqrt{\sum_{\ell,h,w} \alpha(h) \tilde{\hat{x}}_{\ell hw}^2}}, \quad (12)$$

where $\alpha(h) = \cos(h) / (\frac{1}{H} \sum_{h'=1}^H \cos(h'))$ compensates for unequal grid areas across latitudes. The anomaly terms are defined as $\tilde{y}_{\ell hw} = y_{\ell hw} - C$ and $\tilde{\hat{x}}_{\ell hw} = \hat{x}_{\ell hw} - C$, with $C = \frac{1}{LHW} \sum_{\ell,h,w} y_{\ell hw}$ representing the climatological mean.

RMSE reflects the average magnitude of prediction errors while accounting for the Earth’s geometry. ACC instead measures the similarity between predicted and observed anomalies, emphasizing the model’s ability to capture dynamical patterns rather than absolute values. Together, these two metrics provide a balanced view of both error magnitude and anomaly-tracking skill.

E MORE IMPLEMENTATION DETAILS

All experiments are conducted on a server equipped with 8 NVIDIA A100 GPUs. Our implementation of **STORM** is based on PyTorch 2.1.0 (Paszke et al., 2019). For optimization, we adopt the Adam optimizer (Kingma, 2014) with a learning rate of 1×10^{-3} and mean squared error (L2) as the training objective. Each model is trained for 100 epochs with early stopping based on the validation loss. The multi-scale hierarchy is constructed with $M = 3$ levels, and the hidden dimension is fixed to $D = 256$ across all experiments. The *Scale-Bridging Spatio-Temporal Encoder* is composed of $N = 3$ stacked layers. To ensure fairness, all baselines are re-trained under the same data preprocessing, optimization, and training protocols. The model is trained using the mean squared error (MSE) loss between predicted and observed atmospheric states, which aligns with the RMSE evaluation metric and encourages accurate recovery of both large-scale patterns and fine-grained variations.

F EFFICIENCY ANALYSIS

As shown in Table 5, STORM delivers a substantially better efficiency–accuracy trade-off compared with existing data-driven weather models. Despite having only 15.8M parameters, STORM achieves the lowest inference latency (0.87s per 100 samples) and competitive FLOPs, while also attaining the highest prediction accuracy (ACC = 0.984). In contrast, large-scale models such as Pangu and Fuxi incur significantly higher computational and memory costs but still fall short in accuracy. These results highlight that STORM’s lightweight architecture effectively preserves predictive skill while enabling fast and resource-efficient forecasting.

Table 5: Efficiency comparison across representative data-driven weather models.

Metric	STORM	Pangu	FCN	Fuxi
Inference Time ↓ (Seconds / 100 Samples)	0.87	5.11	6.99	19.37
Peak GPU Memory ↓ (MB, Batch Size = 1)	729.22	408.75	265.95	2533.25
Parameters ↓ (M)	15.77	97.48	64.65	661.01
FLOPs ↓ (GFLOPs)	84.59	91.26	58.50	302.46
ACC ↑	0.984	0.952	0.933	0.950

G FULL SENSITIVE ANALYSIS

Table 5 summarizes the scaling behavior of STORM under varying branch numbers and model widths. Increasing either the branch depth or d_{model} consistently improves accuracy, with ACC rising from 0.941 (1 branch, 64 hidden units) to 0.988 (5 branches, 256–512 units), while RMSE steadily decreases. Notably, these gains come with only moderate growth in FLOPs and inference time, indicating that STORM’s multi-branch temporal encoder scales efficiently. The results highlight a clear efficiency–accuracy trend: larger branches yield stronger predictive skill without incurring prohibitive computational cost.

Table 6: Scaling and efficiency analysis of STORM across different branch configurations.

Branch	d_{model}	Total Params	Temp. Enc. Params	FLOPs	Time	Max Mem.	ACC	RMSE
1	64	0.32	2.96E-04	3.17	0.28	13.75	0.941	16.415
1	128	1.20	2.96E-04	11.04	0.30	17.44	0.951	16.323
1	256	4.59	2.96E-04	40.88	0.30	30.01	0.954	16.267
1	512	17.96	2.96E-04	156.92	0.30	82.59	0.958	16.177
2	64	0.64	5.92E-04	4.46	0.56	14.97	0.963	16.136
2	128	2.45	5.92E-04	16.00	0.56	24.43	0.966	16.115
2	256	9.59	5.92E-04	60.32	0.56	51.66	0.971	16.093
2	512	37.92	5.92E-04	233.92	0.59	164.49	0.974	15.983
3	64	1.03	8.88E-04	6.05	0.86	19.48	0.977	15.913
3	128	4.00	8.88E-04	22.16	0.85	30.35	0.981	15.854
3	256	15.77	8.88E-04	84.59	0.87	75.48	0.984	15.809
3	512	62.60	8.88E-04	330.25	0.87	257.33	0.985	15.798
4	64	1.46	1.18E-03	7.44	1.15	20.31	0.979	15.841
4	128	5.70	1.18E-03	27.61	1.16	37.27	0.983	15.813
4	256	22.54	1.18E-03	106.12	1.17	101.06	0.987	15.769
4	512	89.64	1.18E-03	415.84	1.20	360.60	0.986	15.784
5	64	1.96	1.48E-03	8.23	1.49	335.52	0.983	15.808
5	128	7.69	1.48E-03	30.62	1.52	361.66	0.984	15.796
5	256	30.49	1.48E-03	117.84	1.51	448.31	0.988	15.757
5	512	121.40	1.48E-03	462.11	1.53	908.50	0.988	15.716

H MORE DETAILS OF ABLATION ANALYSIS

Tables 7 and 8 highlight the contribution of message passing and scale heterogeneity in STORM’s multi-branch architecture. First, enabling message passing consistently boosts performance across all branch counts, with ACC improvements of 0.6–1.0% and reduced RMSE, indicating more effective cross-scale information flow. Second, branches configured with different temporal scales significantly outperform those using identical scales, showing clear gains that grow with larger branch numbers. These results confirm that both cross-scale communication and scale diversity are essential for extracting complementary temporal patterns and achieving stronger predictive skill.

Table 7: Ablation on message passing across multi-scale branches.

Branch (Scale Numbers)	ACC (with MP)	RMSE (with MP)	ACC (without MP)	RMSE (without MP)
2	0.971	16.093	0.963	16.145
3	0.984	15.809	0.976	15.948
4	0.987	15.769	0.981	15.886
5	0.988	15.757	0.980	16.879

Table 8: Effect of different vs same multi-branch designs.

Scale Number	ACC (Diff Scale)	RMSE (Diff)	ACC (Same Scale)	RMSE (Same)
2	0.971	16.093	0.939	16.547
3	0.984	15.809	0.948	16.382
4	0.987	15.769	0.954	16.285
5	0.988	15.757	0.957	16.179

I FORECAST VISUALIZATION

I.1 MEAN SEA LEVEL PRESSURE (MSLP)

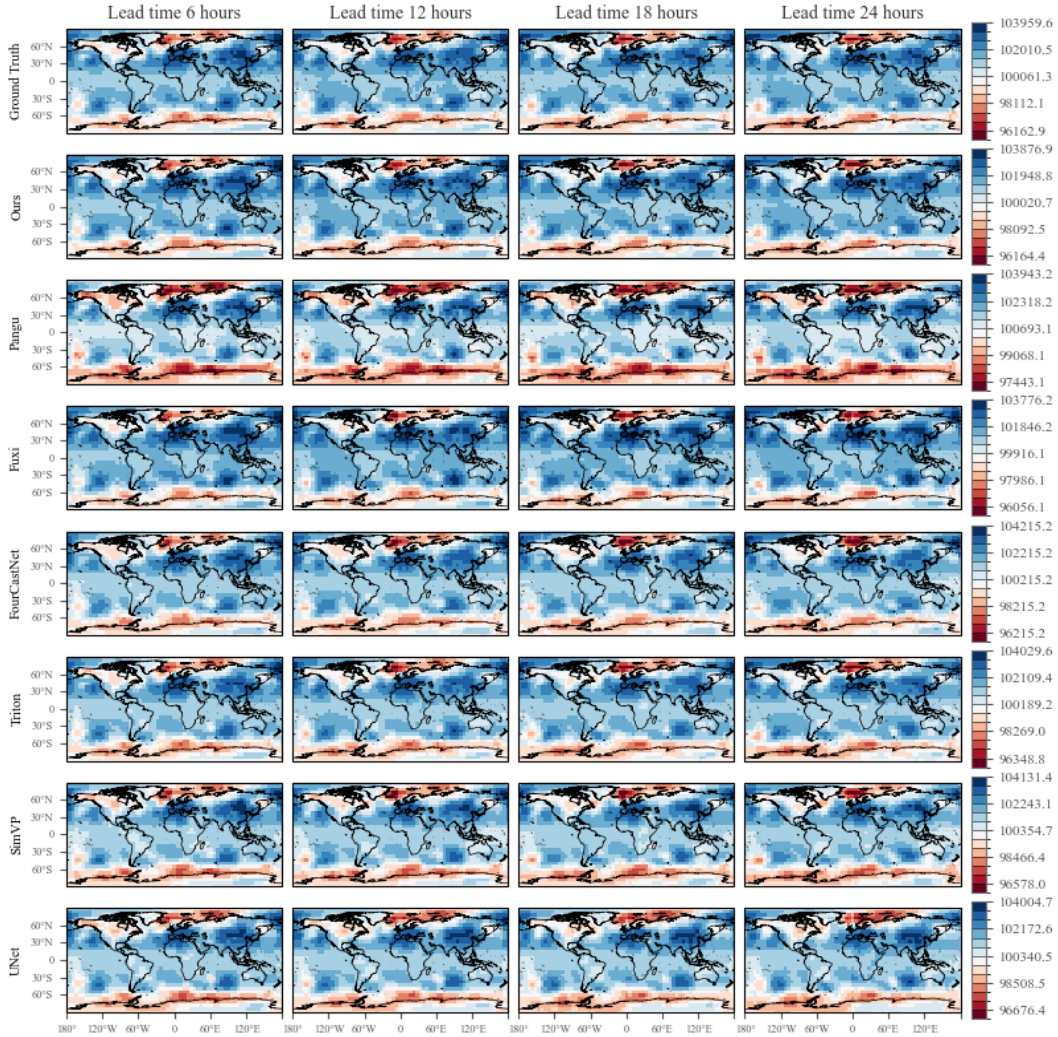


Figure 8: 24-hour forecast results of different models for mean sea level pressure (MSLP).

I.2 SPECIFIC HUMIDITY AT 500 hPa (Q500)

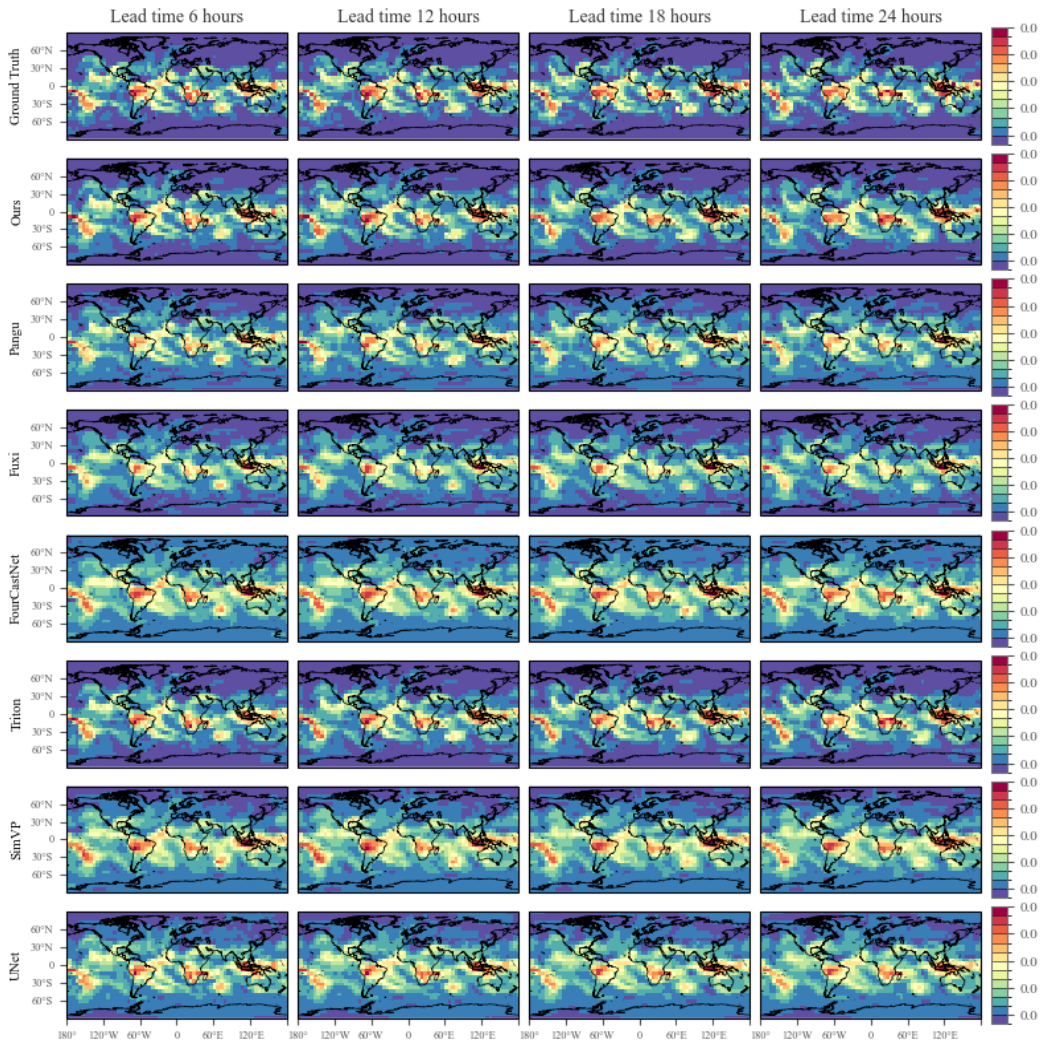


Figure 9: 24-hour forecast results of different models for 500 hPa specific humidity (Q500).

I.3 PRECIPITATION

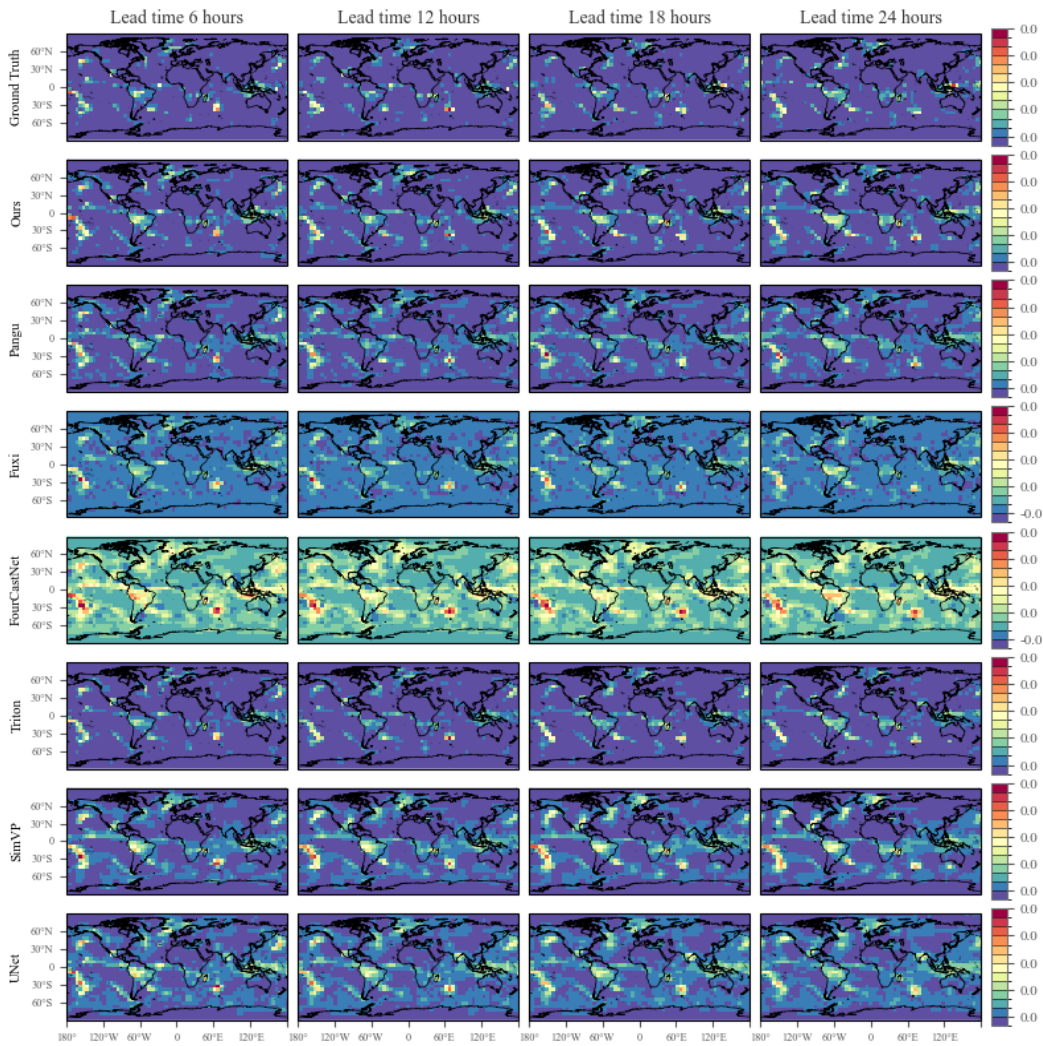


Figure 10: 24-hour precipitation forecast results of different models.

I.4 2-METER TEMPERATURE (T2M)

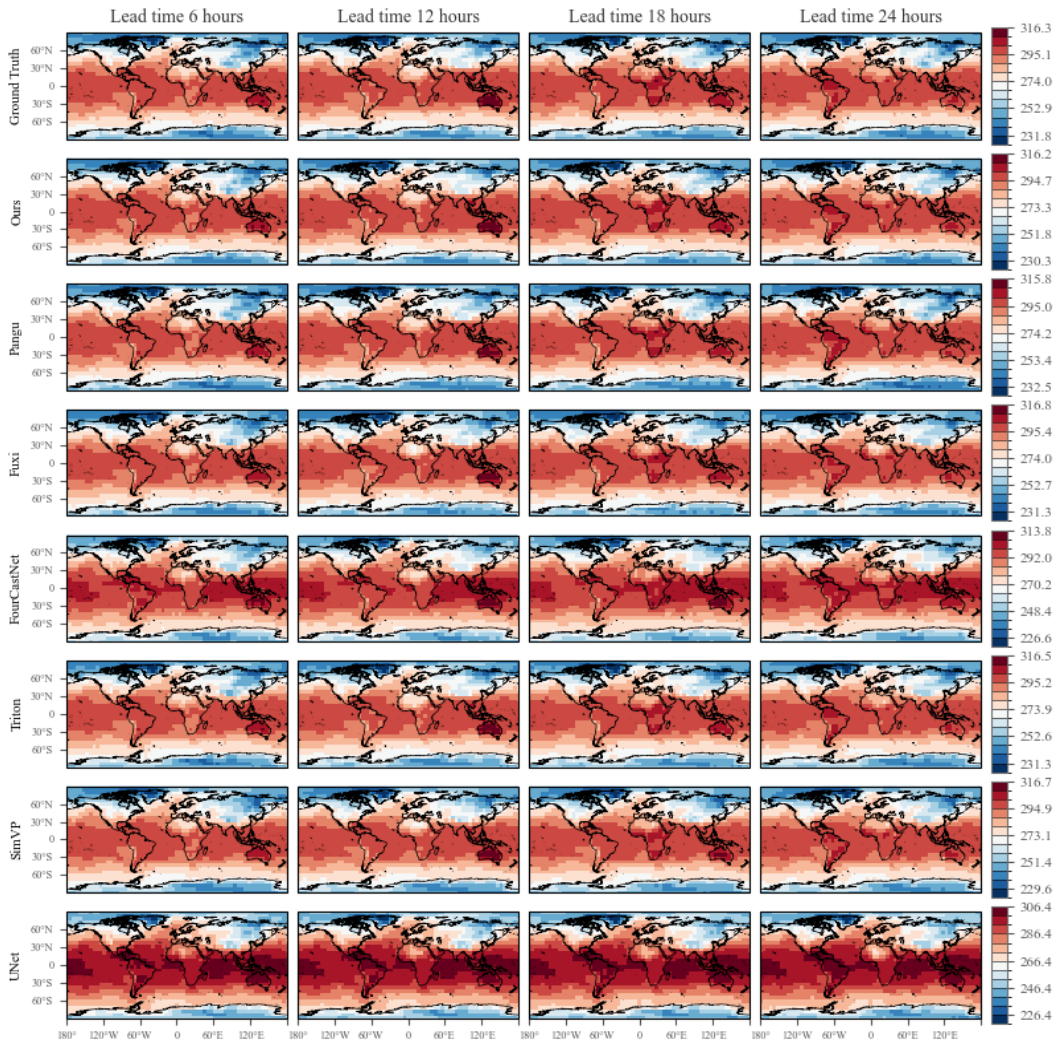


Figure 11: 24-hour forecast results of different models for 2-meter temperature (T2M).

I.5 TEMPERATURE AT 500 hPa (T500)

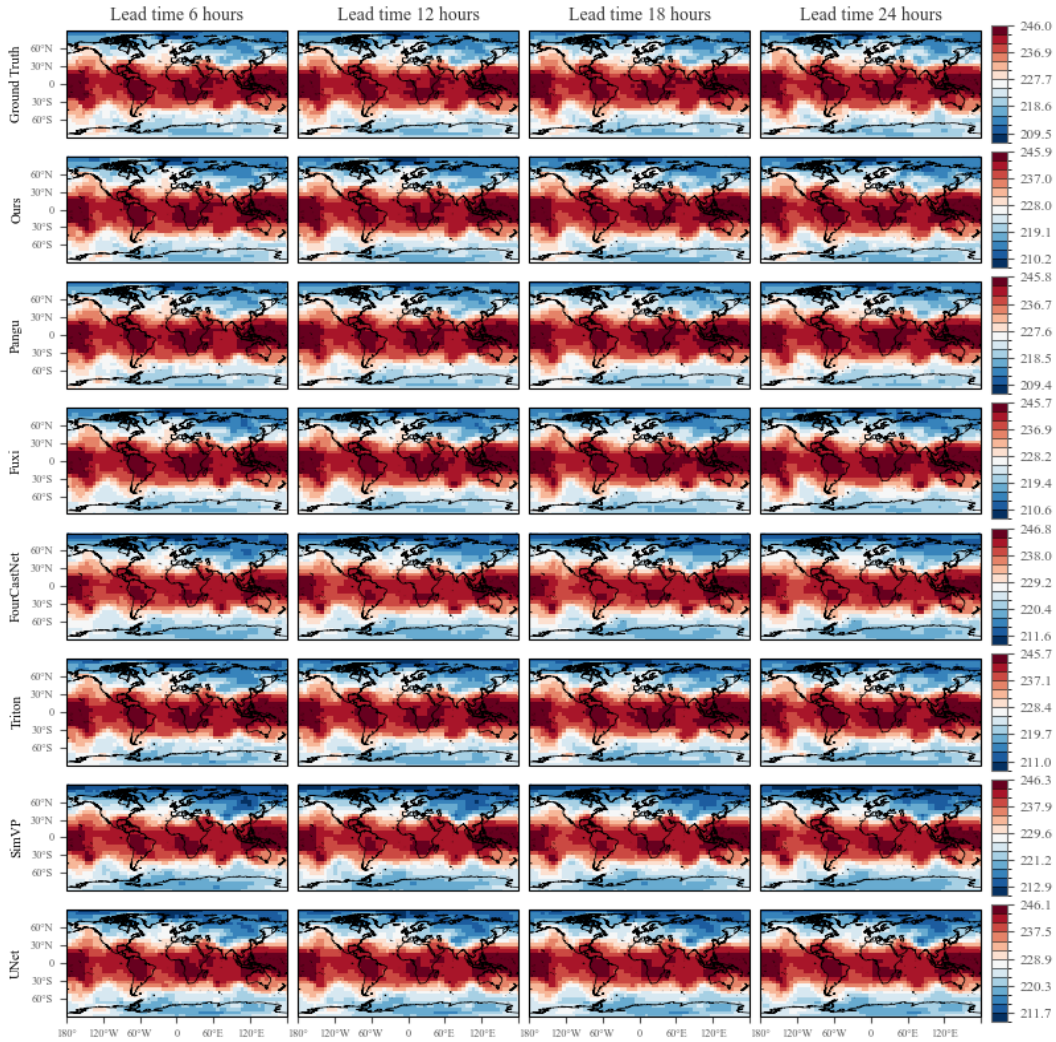


Figure 12: 24-hour forecast results of different models for 500 hPa temperature (T500).

I.6 10-METER ZONAL WIND (U10)

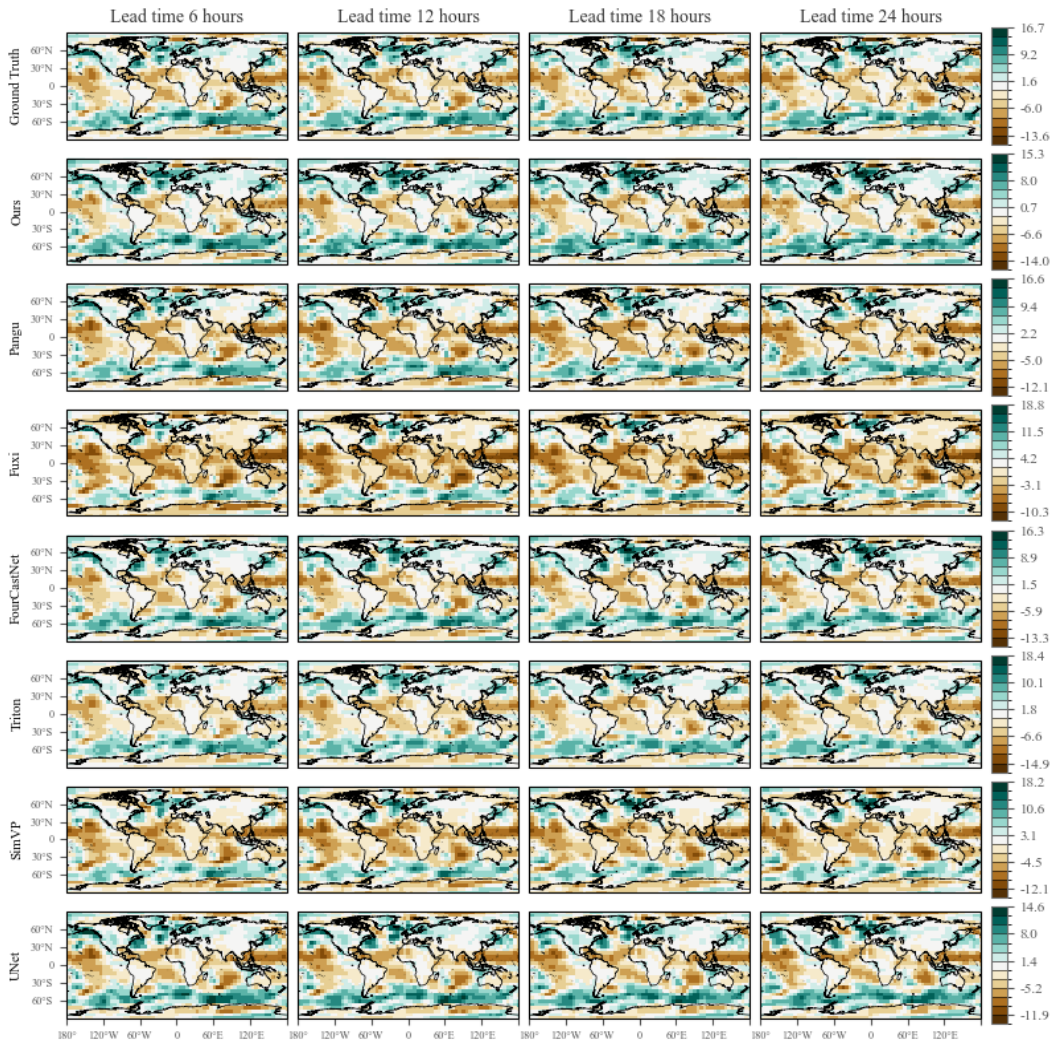


Figure 13: 24-hour forecast results of different models for 10-meter zonal wind (U10).

I.7 ZONAL WIND AT 500 hPa (U500)

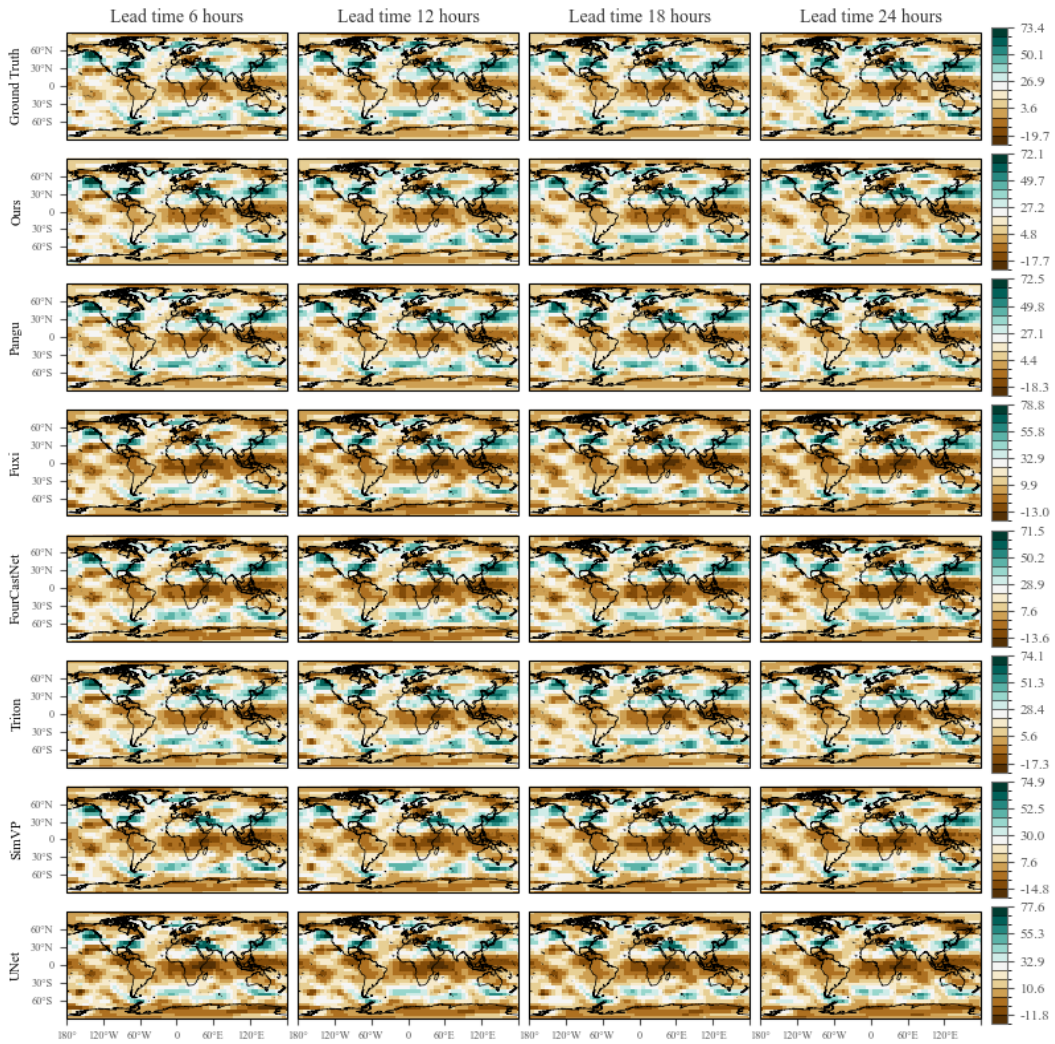


Figure 14: 24-hour forecast results of different models for 500 hPa zonal wind (U500).

I.8 10-METER MERIDIONAL WIND (V10)

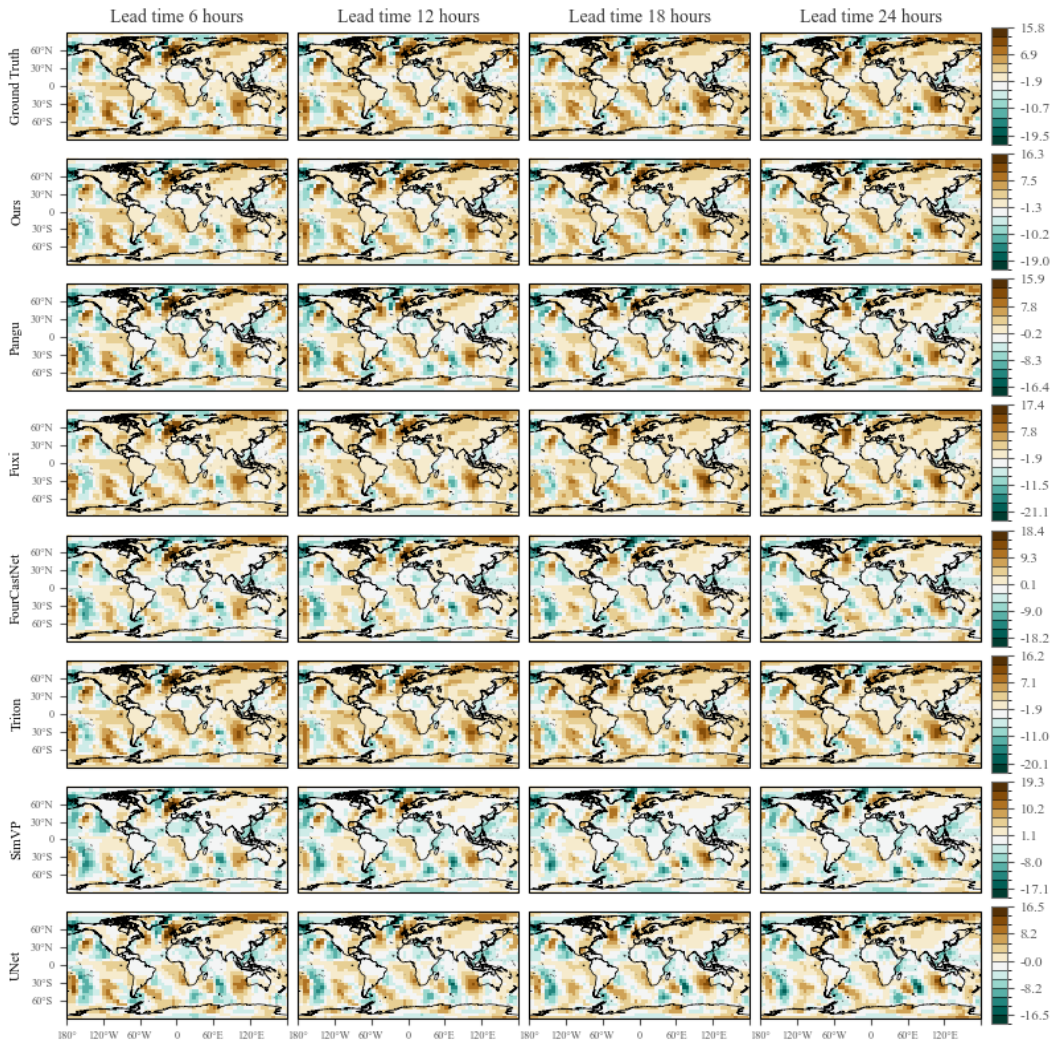


Figure 15: 24-hour forecast results of different models for 10-meter meridional wind (V10).

I.9 MERIDIONAL WIND AT 500 hPa (V500)

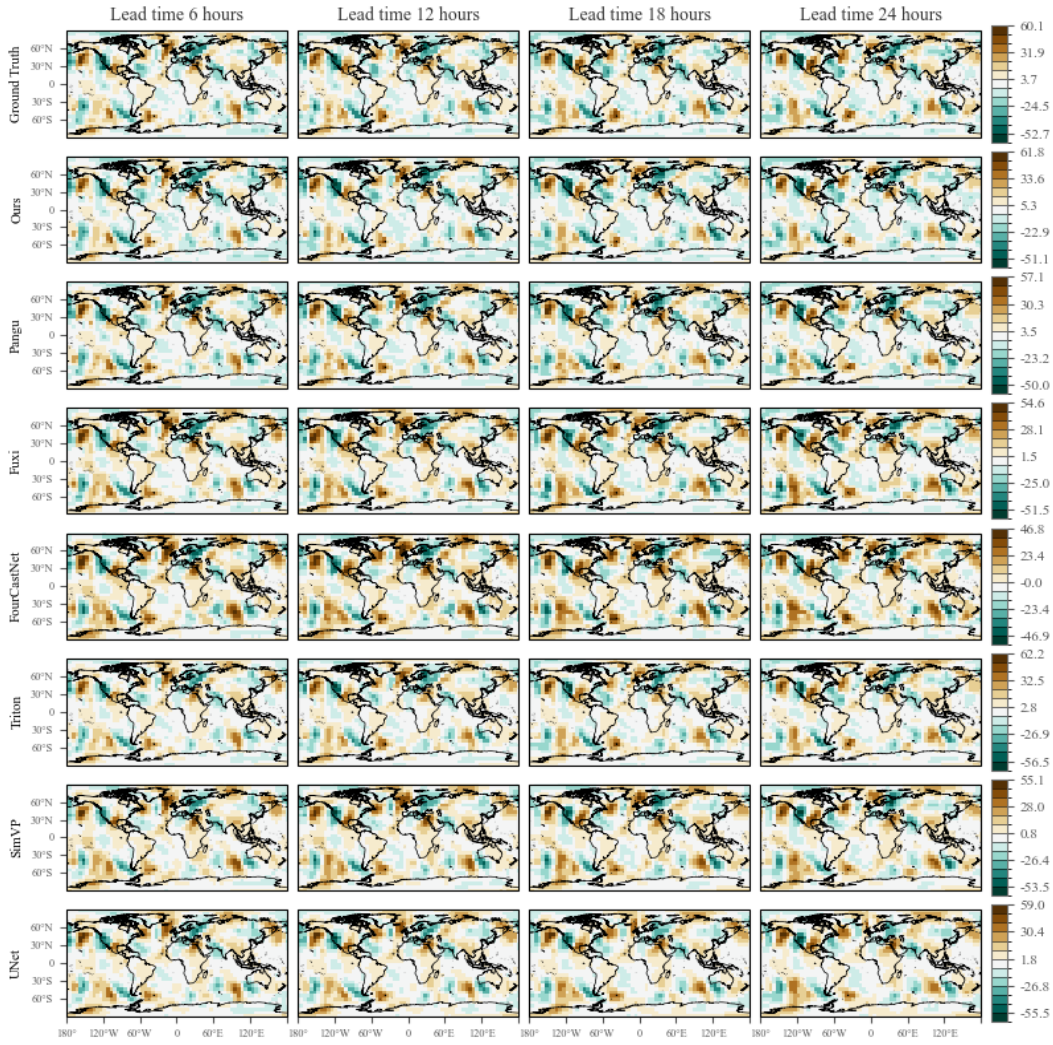


Figure 16: 24-hour forecast results of different models for 500 hPa meridional wind (V500).

I.10 GEOPOTENTIAL HEIGHT AT 500 hPa (Z500)

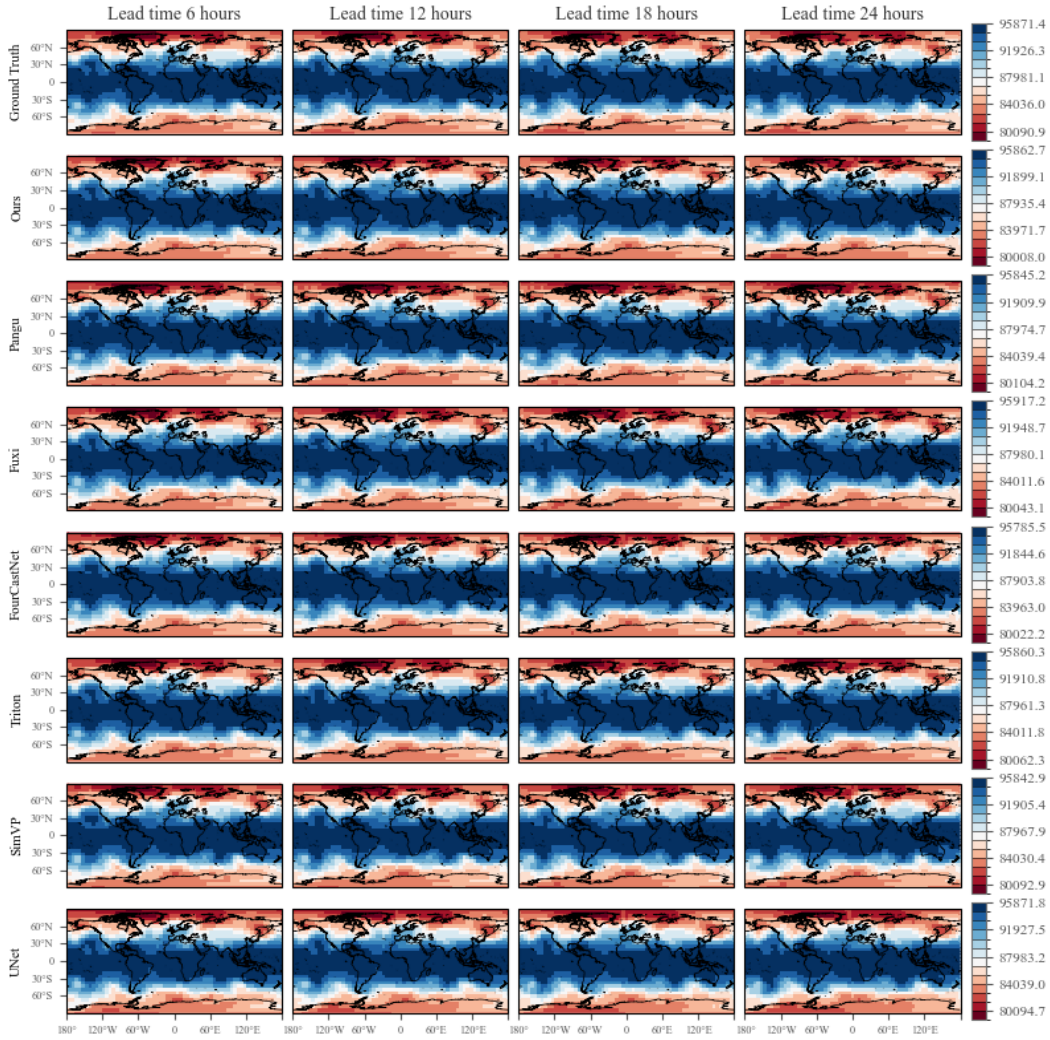


Figure 17: 24-hour forecast results of different models for 500 hPa geopotential height (Z500).

J FULL SHORT-TERM FORECASTING RESULTS.

Table 9: Quantitative comparison of short-term (up to 24 hours) global weather forecasting performance.

Metric		RMSE							ACC						
Variable	Hours	Ours	Triton	Pangu	FCN	Fuxi	SimVP	UNet	Ours	Triton	Pangu	FCN	Fuxi	SimVP	UNet
T2M	6h	0.564	0.718	0.787	1.430	1.191	1.335	1.337	0.999	0.999	0.998	0.995	0.996	0.996	0.995
	12h	0.653	0.836	1.075	1.545	1.308	1.332	2.208	0.999	0.998	0.997	0.994	0.996	0.996	0.987
	18h	0.705	0.929	1.219	1.632	1.415	1.341	2.789	0.999	0.998	0.996	0.993	0.995	0.996	0.982
	24h	0.777	1.010	1.342	1.708	1.513	1.363	3.447	0.998	0.997	0.995	0.993	0.994	0.995	0.981
U10	6h	0.495	0.598	0.775	1.169	0.994	1.279	0.955	0.995	0.993	0.988	0.973	0.981	0.968	0.981
	12h	0.608	0.749	1.209	1.376	1.200	1.359	1.437	0.993	0.989	0.972	0.963	0.972	0.964	0.961
	18h	0.719	0.894	1.590	1.646	1.423	1.497	2.032	0.990	0.985	0.951	0.947	0.961	0.956	0.942
	24h	0.853	1.034	1.933	1.926	1.637	1.659	3.462	0.986	0.979	0.927	0.927	0.948	0.946	0.924
V10	6h	0.520	0.629	0.834	1.274	1.064	1.378	1.012	0.992	0.988	0.979	0.950	0.965	0.941	0.967
	12h	0.647	0.796	1.304	1.492	1.268	1.467	1.491	0.987	0.981	0.947	0.930	0.950	0.933	0.933
	18h	0.768	0.950	1.713	1.782	1.490	1.608	1.994	0.982	0.973	0.908	0.899	0.932	0.919	0.898
	24h	0.917	1.098	2.082	2.084	1.703	1.772	2.971	0.974	0.963	0.862	0.861	0.911	0.900	0.863
Prec	6h	4.2E-04	4.8E-04	6.1E-04	9.2E-04	7.4E-04	9.2E-04	6.7E-04	0.955	0.941	0.906	0.763	0.856	0.768	0.885
	12h	4.9E-04	5.8E-04	7.9E-04	9.5E-04	8.2E-04	9.3E-04	8.9E-04	0.938	0.913	0.833	0.748	0.819	0.758	0.792
	18h	5.9E-04	7.0E-04	9.3E-04	1.0E-03	9.2E-04	9.7E-04	1.1E-03	0.911	0.872	0.765	0.717	0.768	0.737	0.719
	24h	6.6E-04	7.8E-04	1.0E-03	1.1E-03	1.0E-03	1.0E-03	1.4E-03	0.886	0.839	0.705	0.682	0.722	0.713	0.663
MSLP	6h	46.808	60.493	101.678	147.757	112.764	154.169	113.815	0.999	0.999	0.996	0.991	0.995	0.990	0.994
	12h	61.834	82.905	179.577	186.644	148.871	168.679	198.949	0.998	0.997	0.987	0.986	0.991	0.989	0.984
	18h	78.448	104.797	255.410	238.317	188.986	194.126	289.322	0.998	0.996	0.973	0.977	0.986	0.985	0.971
	24h	99.948	126.514	326.712	295.758	229.717	226.092	427.862	0.996	0.994	0.956	0.964	0.979	0.979	0.956
U500	6h	1.384	1.835	1.879	3.540	2.953	3.553	2.503	0.996	0.994	0.993	0.976	0.983	0.976	0.987
	12h	1.713	2.287	2.972	4.148	3.612	3.789	3.880	0.994	0.990	0.983	0.967	0.975	0.973	0.971
	18h	2.041	2.725	3.945	4.940	4.303	4.204	5.158	0.992	0.986	0.970	0.953	0.965	0.966	0.955
	24h	2.472	3.151	4.845	5.802	4.980	4.719	7.166	0.988	0.981	0.955	0.935	0.953	0.957	0.939
V500	6h	1.449	1.873	2.036	3.765	3.155	3.823	2.868	0.992	0.987	0.985	0.947	0.963	0.945	0.969
	12h	1.835	2.367	3.228	4.486	3.817	4.093	4.259	0.987	0.979	0.961	0.924	0.946	0.936	0.933
	18h	2.221	2.843	4.290	5.418	4.500	4.530	5.508	0.982	0.970	0.930	0.887	0.925	0.922	0.897
	24h	2.714	3.305	5.284	6.414	5.169	5.073	7.363	0.972	0.960	0.893	0.841	0.902	0.901	0.859
T500	6h	0.376	0.518	0.513	1.087	0.903	1.189	0.679	0.999	0.998	0.998	0.993	0.995	0.992	0.997
	12h	0.478	0.646	0.802	1.177	1.036	1.210	1.087	0.999	0.998	0.996	0.992	0.994	0.991	0.993
	18h	0.566	0.760	1.024	1.300	1.182	1.255	1.410	0.998	0.997	0.994	0.990	0.992	0.991	0.988
	24h	0.675	0.861	1.207	1.441	1.321	1.313	1.773	0.997	0.996	0.991	0.988	0.990	0.990	0.985
Z500	6h	51.5	68.4	102.6	189.0	142.3	186.4	131.0	1.000	1.000	1.000	0.999	0.999	0.999	0.999
	12h	66.3	93.4	184.6	223.6	185.5	200.9	233.4	1.000	1.000	0.999	0.999	0.999	0.999	0.998
	18h	86.5	122.5	267.1	289.9	238.5	231.9	348.0	1.000	1.000	0.998	0.997	0.998	0.998	0.996
	24h	114.9	153.3	348.5	371.5	294.8	274.6	520.8	1.000	0.999	0.996	0.996	0.997	0.998	0.995
Q500	6h	2.8E-05	3.7E-05	3.4E-05	6.5E-05	5.8E-05	7.5E-05	4.3E-05	0.988	0.979	0.983	0.936	0.949	0.914	0.972
	12h	3.7E-05	4.6E-05	5.2E-05	7.0E-05	6.5E-05	7.5E-05	6.5E-05	0.980	0.968	0.960	0.926	0.935	0.913	0.937
	18h	4.3E-05	5.4E-05	6.4E-05	7.5E-05	7.3E-05	7.7E-05	8.1E-05	0.972	0.956	0.937	0.912	0.918	0.908	0.906
	24h	4.9E-05	6.0E-05	7.4E-05	8.1E-05	8.0E-05	7.9E-05	1.0E-04	0.963	0.945	0.916	0.897	0.900	0.902	0.881

K FULL LONG-TERM FORECASTING RESULTS.

Table 10: Quantitative comparison of long-term (7–10 days) global weather forecasting performance.

Metric		RMSE							ACC						
Variable	Days	Ours	Triton	Pangu	FCN	Fuxi	SimVP	UNet	Ours	Triton	Pangu	FCN	Fuxi	SimVP	UNet
T2M	7d	2.293	<u>2.934</u>	3.423	3.902	3.294	2.938	4.051	0.987	0.974	0.963	0.975	0.973	<u>0.979</u>	0.948
	8d	2.516	3.263	3.574	4.104	3.442	<u>3.100</u>	4.358	0.985	0.968	0.958	0.971	0.970	<u>0.977</u>	0.940
	9d	2.708	3.549	3.712	4.288	3.574	<u>3.248</u>	4.630	0.982	0.961	0.952	0.969	0.968	<u>0.974</u>	0.933
	10d	2.865	3.799	3.821	4.430	3.689	<u>3.384</u>	4.867	0.981	0.956	0.948	0.967	0.966	<u>0.972</u>	0.928
U10	7d	3.485	3.945	4.959	5.102	4.528	<u>3.766</u>	5.507	0.769	0.700	0.663	0.645	0.608	<u>0.707</u>	0.606
	8d	3.773	4.192	5.088	5.301	4.660	<u>3.872</u>	5.753	0.730	0.662	0.627	0.614	0.582	<u>0.689</u>	0.567
	9d	3.954	4.397	5.192	5.464	4.762	<u>3.997</u>	5.953	0.697	0.631	0.597	0.588	0.561	<u>0.675</u>	0.541
	10d	4.013	4.548	5.268	5.583	4.834	<u>4.174</u>	6.099	0.670	0.606	0.572	0.568	0.544	<u>0.664</u>	0.524
V10	7d	3.787	4.205	4.961	5.364	4.652	<u>3.982</u>	5.757	0.559	<u>0.451</u>	0.392	0.358	0.326	0.427	0.306
	8d	4.089	4.445	5.069	5.514	4.764	<u>4.098</u>	5.986	0.486	0.388	0.342	0.310	0.291	<u>0.391</u>	0.271
	9d	4.154	4.620	5.150	5.649	4.853	<u>4.335</u>	6.158	0.426	0.339	0.299	0.274	0.264	<u>0.366</u>	0.244
	10d	4.201	4.747	5.201	5.749	4.911	<u>4.500</u>	6.277	0.383	0.302	0.266	0.247	0.245	<u>0.349</u>	0.225
Prec	7d	1.3E-03	1.9E-03	1.7E-03	1.5E-03	1.6E-03	<u>1.4E-03</u>	2.2E-03	0.492	0.354	0.329	0.259	0.271	<u>0.396</u>	0.242
	8d	1.4E-03	2.1E-03	1.8E-03	1.6E-03	1.6E-03	<u>1.5E-03</u>	2.3E-03	0.446	0.316	0.297	0.231	0.249	<u>0.384</u>	0.211
	9d	1.4E-03	2.2E-03	1.8E-03	1.6E-03	1.7E-03	<u>1.5E-03</u>	2.3E-03	0.410	0.287	0.272	0.210	0.233	<u>0.376</u>	0.190
	10d	1.4E-03	2.3E-03	1.8E-03	1.6E-03	1.7E-03	<u>1.6E-03</u>	2.4E-03	0.381	0.262	0.252	0.193	0.220	<u>0.370</u>	0.173
MSLP	7d	640.6	<u>731.4</u>	1075.0	969.2	901.1	741.8	1067.9	0.835	0.779	<u>0.785</u>	0.764	0.680	0.770	0.733
	8d	713.0	795.5	1114.5	1024.9	940.6	<u>775.8</u>	1128.5	0.796	0.738	<u>0.754</u>	0.730	0.650	0.748	0.695
	9d	771.7	847.9	1145.0	1069.5	969.0	<u>801.4</u>	1181.0	0.762	0.706	0.725	0.701	0.627	<u>0.730</u>	0.660
	10d	816.2	887.7	1166.9	1101.8	989.2	<u>820.0</u>	1220.0	0.734	0.678	0.700	0.678	0.608	<u>0.716</u>	0.630
U925	7d	5.661	7.696	10.090	8.300	9.408	<u>7.572</u>	11.118	0.915	0.839	0.842	0.833	0.782	<u>0.848</u>	0.796
	8d	6.320	8.590	10.607	8.936	9.972	<u>7.972</u>	12.066	0.894	0.802	0.816	0.808	0.756	<u>0.832</u>	0.763
	9d	6.911	9.354	11.050	9.477	10.426	<u>8.313</u>	12.659	0.874	0.769	0.789	0.779	0.734	<u>0.819</u>	0.730
	10d	7.436	10.031	11.430	9.921	10.803	<u>8.611</u>	13.103	0.854	0.739	0.765	0.752	0.716	<u>0.807</u>	0.699
V925	7d	5.674	7.095	9.228	8.929	8.310	<u>6.765</u>	10.013	0.643	<u>0.485</u>	0.395	0.376	0.289	0.416	0.300
	8d	6.344	7.733	9.602	9.466	8.704	<u>7.061</u>	10.684	0.556	<u>0.397</u>	0.323	0.307	0.226	0.355	0.223
	9d	6.923	8.210	9.892	9.880	8.981	<u>7.294</u>	11.174	0.474	<u>0.327</u>	0.263	0.250	0.183	0.305	0.166
	10d	7.412	8.603	10.105	10.198	9.182	<u>7.473</u>	11.560	0.402	<u>0.268</u>	0.214	0.204	0.151	0.266	0.131
T925	7d	2.420	<u>3.251</u>	4.015	3.496	4.163	3.333	4.872	0.975	<u>0.952</u>	0.944	0.949	0.925	0.952	0.920
	8d	2.690	3.585	4.232	3.777	4.421	<u>3.504</u>	5.204	0.969	0.942	0.935	0.942	0.916	<u>0.947</u>	0.908
	9d	2.932	3.882	4.420	4.022	4.642	<u>3.649</u>	5.523	0.963	0.932	0.926	0.934	0.908	<u>0.943</u>	0.896
	10d	3.145	4.152	4.566	4.223	4.827	<u>3.774</u>	5.724	0.957	0.922	0.917	0.926	0.901	<u>0.939</u>	0.884
Z925	7d	3.0E-07	4.7E-07	4.2E-07	4.3E-07	5.2E-07	<u>3.8E-07</u>	5.8E-07	0.782	0.611	0.607	0.620	0.567	<u>0.653</u>	0.565
	8d	3.2E-07	5.2E-07	4.4E-07	4.6E-07	5.5E-07	<u>3.9E-07</u>	6.3E-07	0.760	0.573	0.571	0.586	0.544	<u>0.637</u>	0.524
	9d	3.3E-07	5.6E-07	4.6E-07	4.8E-07	5.7E-07	<u>4.1E-07</u>	6.6E-07	0.738	0.537	0.537	0.554	0.524	<u>0.622</u>	0.504
	10d	3.5E-07	6.0E-07	4.8E-07	5.0E-07	5.8E-07	<u>4.2E-07</u>	6.8E-07	0.717	0.502	0.509	0.527	0.506	<u>0.609</u>	0.482
Q925	7d	673.038	871.088	1311.785	<u>836.431</u>	1172.687	989.917	1394.336	0.987	0.973	0.966	0.973	0.966	<u>0.975</u>	0.947
	8d	773.302	999.146	1391.247	<u>928.037</u>	1270.395	1067.484	1499.221	0.983	0.964	0.958	0.965	0.960	<u>0.972</u>	0.938
	9d	863.541	1113.102	1459.822	<u>1017.677</u>	1351.076	1135.576	1591.308	0.979	0.955	0.951	0.958	0.956	<u>0.969</u>	0.931
	10d	943.733	1214.456	1513.909	<u>1093.027</u>	1422.259	1196.480	1666.658	0.975	0.946	0.946	0.954	0.951	<u>0.966</u>	0.926